Mobility Studies on Siloxane–Based Inorganic–Organic Hybrid Polymers by High Resolution Solid and Suspension State NMR Techniques

and

Analysis of Dynamic Parameters Derived by NMR Spectroscopy via a Neural Network

***

Mobilitätsstudien an anorganisch–organischen Hybridpolymeren auf Siloxanbasis mittels Techniken der hochauflösenden Festkörper– und Suspensions–NMR–Spektroskopie

und

Analyse NMR–spektroskopisch ermittelter dynamischer Parameter mit Hilfe eines Neuronalen Netzwerkes

DISSERTATION

der Fakultät für Chemie und Pharmazie
der Eberhard–Karls–Universität Tübingen

zur Erlangung des Grades eines Doktors
der Naturwissenschaften

2001

vorgelegt von

Frank Höhn

Tag der mündlichen Prüfung:	21.12.2000
Dekan:	Prof. Dr. H. Probst
1. Berichterstatter:	Prof. Dr. E. Lindner
2. Berichterstatter:	Prof. Dr. H. A. Mayer

Die vorliegende Arbeit wurde am

Institut für Anorganische Chemie II der

Eberhard–Karls–Universität Tübingen

unter der Leitung von Prof. Dr. rer. nat. Ekkehard Lindner

angefertigt.

Meinem Doktorvater

Herrn Prof. Dr. Ekkehard Lindner,

danke ich herzlich für die interessante Themenstellung,

die Bereitstellung ausgezeichneter Arbeitsbedingungen,

für wertvolle Anregungen und Diskussionen

sowie für sein stetes Interesse an dieser Arbeit.

Für meine Eltern, für Elke und meinen Bruder

Mein herzlicher Dank gilt Herrn Priv.–Doz. Dr. Hermann A. Mayer für die in allen Belangen freundschaftliche Zusammenarbeit und stete Hilfsbereitschaft, zahlreiche fruchtbare Diskussionen sowie Zuspruch und Motivation in Stunden der wissenschaftlichen Not.

Herrn Prof. Dr. Klaus Albert und allen Mitgliedern seines Arbeitskreises danke ich für die gute Kooperation in der NMR Abteilung.

Herrn Dipl.–Inform. Thomas Hermle danke ich für die gute Zusammenarbeit, das geduldige Anfertigen einer Vielzahl von Kohonen Karten und das Ertragen von noch mehr Änderungswünschen.

Ich danke den 'Festkörper–NMR–Spektroskopikern' Dr. Andreas Baumann, Dr. Joachim Büchele, Dr. Andreas Jäger und Dr. Theodor Schneller für wichtige und richtige Antworten auf viele Fragen zur Spektrometerbedienung und vor allem Herrn Walter Schaal für die Hilfsbereitschaft und das fachkundige Behandeln kranker Geräte in den Festkörper–NMR Stationen.

Herrn Dr. Klaus Eichele möchte ich für die ständige Bereitschaft zu hilfreichen Diskussionen über alle Aspekte der NMR Spektroskopie danken.

Frau Dr. Monika Förster danke ich für die Freundschaft im und um das Labor, ihrem 'eigenen' (guten!) Geschmack in Layoutfragen, harte Begegnungen im Squash–Court und nicht zu knapp für moralische Unterstützung.

Den ehemaligen 'Labormitinsassen' von 8M14 Dipl. Chem. Christoph Ayasse, Dr. Matthias Günther, M. Sc. Monther Khanfar, Dr. Stefan Pautz und Dr. Markus Schmid für ein ausgezeichnetes Arbeitsklima, wertvolle Diskussionen (sinniger und manchmal unsinniger Themen) am Abzug und viele Glasgeräte.

Den Herren M. Sc. Monther Khanfar, Dr. Markus Schmid, Dr. Robert Veigel und Dr. Joachim Wald 'danke' ich für "Erholung" im Computerraum und am Billardtisch.

Ferner möchte ich den Mitgliedern der Montags–Fußballgruppe M. Sc. Samer Al–Gharabli, Dipl. Chem. Christoph Ayasse, Dipl. Ing. FH Stefan Brugger, Dr. Matthias Günther, Dr.

Thomas Leibfritz, Dr. Markus Mohr, Dipl. Chem. Thomas Salesch, Dr. Joachim Wald und M. Sc. Ruifa Zong für das Aufhalten gegnerischer Konter, Steilpässe und meistens schmerzfreies Fußballspielen danken.

Des weiteren danke ich Frau Roswitha Conrad, Frau Heike Dorn, Herrn Dr. Hans–Dieter Ebert, Frau Angelika Ehmann, Frau Barbara Saller und allen anderen technischen und wissenschaftlichen Angestellten, die am Gelingen dieser Dissertation Anteil hatten, für die gute Zusammenarbeit und die freundschaftliche Atmosphäre im Arbeitskreis.

Nicht zuletzt möchte ich mich bei allen anderen, nichtgenannten Kolleginnen und Kollegen der Arbeitskreise Kuhn, Lindner, Mayer und Nagel für das gute Klima in der Anorganik II, die ständige (gefragte und nicht gefragte) Diskussionsbereitschaft und für viele erholsame Stunden im Kaffeeraum und in der Cafeteria danken.

Mein ganz besonderer persönlicher Dank gilt meiner Freundin Elke, die mich auch in den schwersten Momenten immer getragen und damit den größten moralischen Beitrag zum Gelingen dieser Doktorarbeit geleistet hat.

Contents

1. Introduction 1

2. General Section – Materials and Methods 5

2.1. Materials and Methods 5
2.1.1. Materials 5
2.1.2. Methods 6
2.1.2.1. Solid State NMR Spectroscopy 6
2.1.2.2. Suspended State NMR Spectroscopy 9
2.1.2.3. Dynamic Deuterium NMR Spectroscopy 10
2.1.2.4. Computational Methods 11

3. General Section – Discussion 22

3.1. Mobility Studies on Inorganic–Organic Hybrid Polymers 22
3.1.1. ^{29}Si CP/MAS NMR Spectroscopy 22
3.1.2. ^{13}C and ^{31}P CP/MAS NMR Spectroscopy 25
3.1.3. Temperature Dependent $T_{1\rho H}$ Measurements 28
3.1.4. Dynamic ^{2}H NMR Spectroscopy 33
3.1.5. ^{1}H HR/MAS and ^{13}C CP/MAS NMR Spectroscopy in the Suspended State . 35
3.1.6. Dynamic ^{1}H SPE/MAS NMR Spectroscopy 40

3.2. Evaluation of NMR Spectroscopic Derived Dynamic Parameters by Kohonen's Self Organizing Feature Map 48

4. Conclusions 57

4.1. Mobility Studies on Inorganic–Organic Hybrid Polymers 57

4.2. Evaluation of NMR Spectroscopic Derived Dynamic Parameters 57

5. Experimental Section 58

5.1. Solid State NMR Measurements 58

5.2. Suspension State NMR Measurements 58

6. References 67

7. Summary.....67

Abbreviations and Definitions

2D	Two–dimensional
A	Peak area (synonymous with *I*)
ANN	Artificial Neural Network
ART	Adaptive Resonance Theory
ASCII	American Standard Code for Information Interchange
BET	Brunauer–Emmet–Teller (determination of surfaces by adsorption of nitrogen)
CP	Cross–polarization
D	D type silicon atom (two oxygen neighbors)
DCM	Dichloromethane
Et_2O	Diethyl ether
EtOH	Ethanol
EXAFS	Extended X–ray Absorption Fine Structure (spectroscopy)
Fn	Functionality
g	Grams
HPDEC	*H*igh *p*ower *dec*oupling
HR	High resolution
Hz	Hertz
I	Intensity of the NMR signal
K	Kelvin
kHz	Kilohertz
MAS	Magic–Angle–Spinning
MeOH	Methanol
MHz	Megahertz
ms	Millisecond
NMR	Nuclear Magnetic Resonance
PC1	Principle Component 1
PC2	Principle Component 2
PCA	Principle component analysis
PEG	Polyethylene glycol
ppm	Parts per million
Q	Q type silicon atom (four oxygen neighbors)
SOM	Self–Organizing Feature Map

SPE	Single pulse excitation
T	T type silicon atom (three oxygen neighbors)
$T_{1\rho H}$	Proton spin–lattice relaxation time in the rotating frame
T_C	(Hartman–Hahn) Contact time
T_{XH}	Cross–polarization constant of the heteronucleus X
THF	Tetrahydrofuran
WISE	*Wi*deline *Se*paration (NMR spectroscopy)
z	Spacer length (number of methylene units)

Greek Letters:

δ	Chemical shift
µ	Mikro
ν	Frequency
τ	Time delay

For editorial reasons the punctuation signs ′.′ and ′,′ in Tables 2 – 20 and in the diagram containing Figures 8 – 10, 12, and 19 – 24 are used synonymously.

1. Introduction

One of the most important advantages of homogeneous catalysis is the possibility to control conversions and selectivities towards the desired products. The ambition to transfer these properties to supported catalysts in order to facilitate the separation of the reaction products from the catalyst has not been achieved in a satisfactory way. The severe problems of leaching of the catalyst from the polymer backbone have not been solved yet.[1] In addition, the knowledge about the nature of reactive centers is mostly empirical. A considerable improvement of the benefits in the combination of homogeneous and heterogeneous catalysis was obtained by introducing the concept of the interphase, which is derived from reversed phase chromatography.[2–4]

Interphases are systems in which a stationary phase and a mobile component penetrate each other on a molecular scale without forming a homogeneous phase. In ideal interphase regions reactive centers remain highly mobile and simulate the properties of a solution. Simple recovery of catalysts by filtration and a control of activity and selectivity are guaranteed, the leaching is largely reduced, and the reactivity can be modified by the employment of copolymers.[5]

The sol–gel process[6] is a versatile method capable to generate inorganic–organic hybrid polymers with excellent swelling abilities and high accessibility for even large substrates. If transition metal complexes are provided with T–silyl functionalities they can be subjected to a sol–gel process to yield stationary phases.[7] They consist of an inert polysiloxane matrix, a flexible spacer and the reactive center. The mobile phase is a gaseous, liquid or dissolved reactant or simply a solvent. The matrix located transition metal complexes are securely incorporated into the hybrid polymer and sufficient swelling enables the accessibility of the reactive centers.

T–functionalized silanes of the type Fn–Si(OMe)$_3$ serve for the generation of stationary phases, which were subjected to the sol–gel process with or without co–condensing agents.[6–11] The functional group Fn generally represents either a ligand or a complex and is distributed statistically across the entire carrier matrix.

Co–condensing agents are taking over the task to control the density and distance of the reactive centers and to eventually avoid leaching.[6,10,12,13] They are the components which modulate the stationary phase from rigid to highly mobile and are also responsible for the porosity and swelling ability of the material. Frequently applied co–condensing agents are siloxanes such as Si(OEt)$_4$ (**Q^0**),[14–16] MeSi(OMe)$_3$ (**T^0**),[14,15] or Me$_2$Si(OMe)$_2$ (**D^0**).[14,15,17] Although copolymers with D groups reveal the desired high mobility in interphases, they have the disadvantage to be washed out during the sol–gel process. However, copolymers with Q groups are characterized by complementary properties. They are rigidly anchored within the matrix and hence cannot be washed out, but they lack the necessary mobility. By employing D–bifunctionalized silanes of the type Me(MeO)$_2$Si(CH$_2$)$_z$Si(OMe)$_2$Me (**D^0–C$_z$–D^0**) recently the combination of the advantages of D and Q co–condensing agents was successful. The resulting copolymers revealed an optimum of cross–linkage and swelling abilities and cannot be washed out of the polymer matrix.[18–22] Novel specially designed D– and T–functionalized co–condensing agents of the type of R'(MeO)$_2$Si–(CH$_2$)$_z$–(C$_6$R$_4$)–(CH$_2$)$_z$–Si(OMe)$_2$R' (R = H, D; R' = Me, OMe; z = 3, 4) were synthesized in order to further improve the swelling abilities of inorganic–organic polymers and to control possible diffusion problems of large molecules.[23] Very recently similar systems, however, with less methylene units, were published by *Corriu et al.* and *Carr et al.*.[24–28]

As the polymers described above are of completely amorphous nature X–ray crystal structure analysis is not applicable to characterize their structures. The main tool to investigate, characterize, and quantify the inorganic–organic hybrid polymers is the solid

state NMR spectroscopy. The mobilities of polymers in the solid state and in the suspended state, i. e. in a real interphase, can be determined and evaluated by employing dynamic NMR spectroscopic experiments, i.e. relaxation time measurements in the solid and the suspended state.

It is clear that the number of parameters and properties obtained by NMR spectroscopy and other experimental methods (EXAFS, BET, etc) increases with each new material designed. This complicates a comparison of these materials with common analytic and statistic methods. In certain cases Artificial Neural Networks (ANNs) are better suited to undertake this task, in fact they have been successfully used in chemistry for pattern recognition and multivariate data analysis.[29] Since the beginning of the 1980s ANNs have become a rapidly growing field in computer science and at present a wide range of different ANN algorithms and principles are available.[30]

All ANNs acquire knowledge about a certain problem from studying a set of data – called the training data set. Two fundamentally different learning strategies can be applied: supervised and unsupervised learning. In the first case, a set of corresponding correct answers (desired outputs) has to be presented for the training data set. Hence the learning procedure can employ this knowledge (that has to be possessed in advance). One of the best known neural networks, the multi layer perceptron with error backpropagation (BPN) follows this strategy.[31] For unsupervised learning, no prior knowledge is utilized in the training process. All information have to be extracted from the data automatically. Adaptive Resonance Theory Networks (ART) and Kohonen's Self–Organizing Feature Map (SOM) are examples for self–organizing unsupervised neural networks.[32]

In contrast to common statistical methods, ANNs are not restricted to linear correlations or linear subspaces. They can take into account nonlinear structures and structures of arbitrarily shaped clusters or curved manifolds. Therefore they can be applied

effectively and efficiently for classification (identifying objects), prediction (modeling of functional correlation), and visualization (reducing dimensions).

In the first part of this thesis the mobilities of new inorganic–organic hybrid polymers in the solid and in the suspended state will be investigated and correlated with its physical properties, particularly with the resulting cross–linkage. In the second part the application of a non–supervised neural network, the so–called Kohonen's Self Organizing Feature Map (SOM), is described to work as a tool, to visualize structure and similarities in NMR relaxation time data sets, that characterize stationary phases that were synthesized in the work groups of *E. Lindner* and *H. A. Mayer*. The results of this visualization are used to compare inorganic–organic hybrid polymers that comprise different structural features and show different mechanical properties. Based on cross–linkage (T^0 – T^3, D, T, and Q) and NMR relaxation time data (T_{PH}, $T_{1\rho H}$) correlations of these materials are extracted, which were not obvious beforehand.

2. General Section – Materials and Methods

2.1. Materials and Methods

2.1.1. Materials

A perusal of Table 1 shows the diversity of the reactive centers, the spacers and the polysiloxane matrices, which were prepared over the last years.[7,15,22,23,52–55] The phosphine ligands range from bulky to less sterically hindered mono– (**1** – **3**, **36**, **46**), bis– (**70**), and trisphosphines (**49**) linked via one, two, and three hydrocarbon chains of different lengths, respectively, to the polymer. The metal complexes cover the coordination geometries of *cis* and *trans* square planar and octahedral (**28**, **48**, **64**). Moreover the metal centers are connected to one, two, and three phosphines, respectively. The spacers not only differ in their lengths; they also vary in their shape and polarity (alkane, PEG)(**25**, **52**). All these materials have been synthesized by more or less the same hydrolytic sol–gel routes, but following the necessities of solubility of the transition metal complexes, these sol–gel routes differ in the organic solvents employed. Commonly alcohols (MeOH, EtOH) or ethers (THF, Et_2O), rarely CH_2Cl_2 are applied. The utilization of solvents of different polarity in sol–gel processing leads to hybrid polymers with different physical and possibly different mechanical properties. In order to investigate the properties of the polymer matrices in dependence on the solvent for the sol–gel process and the type of the linker (D or T group) new deuterium labeled co–condensing agents have been synthesized.[55] Following two different sol–gel routes, employing MeOH and THF as solvents, respectively, they yield the inorganic–organic hybrid polymers **80** – **83**. In an earlier work similar systems (**73** – **79**) have been prepared for the first time, in order to investigate their suitability as new co–condensing agents with new swelling capabilities.[23]

2.1.2. Methods

2.1.2.1. Solid State NMR Spectroscopy

The inorganic–organic hybrid polymers presented in Table 1, are prepared by hydrolytic sol–gel processes and are of amorphous nature. Thus solid state NMR spectroscopy is *the* ideal tool to reveal structural and dynamic properties of these systems. The application of multinuclear CP/MAS NMR experiments allows the characterization of the structure of the polymer backbone, the local surroundings of the metal centers, and the functional groups of the ligands.[33–35] Considering the polymers introduced in Table 1 commonly the spin ½ nuclei ^{13}C and ^{29}Si – representing the polymer backbone – and ^{31}P – representing the reactive centers – are the subjects of investigations. By determination of dynamic NMR parameters it is possible to quantify the solid state NMR spectra.[7,36] The results of dynamic NMR measurements permit an insight into the degrees of hydrolysis and condensation of the polymer network and the quality of the sol–gel process applied.

In order to monitor the mobility of dry polymers measurements of the proton spin–lattice relaxation time in the rotating frame $T_{1\rho H}$ are a common task.[37] This parameter covers a temporal range of a few milliseconds and corresponds to molecular motions in the kHz region. It is determined by multinuclear (^{13}C, ^{29}Si, or ^{31}P) CP/MAS NMR experiments in which spin lock times are varied. $T_{1\rho H}$ can be calculated by fitting the obtained signal intensities $I(\tau)$ in dependence of the spin-lock time τ of the corresponding nucleus to eq. (1).[38]

$$I(\tau) = I(0)e^{-\frac{\tau}{T_{1\rho H}}} \qquad (1)$$

If the sample polymer is built up homogeneously strong dipole–dipole coupled protons throughout the whole system can be assumed and relaxation should be controlled by a spin–diffusion mechanism.[36,39–41] In that case the determined $T_{1\rho H}$ value will be uniform for all protons throughout the sample.

To obtain precise information about the mobility of molecules or molecular fragments by examining $T_{1\rho H}$ or other relaxation times (e.g. T_1, T_2) the corresponding correlation times τ_R must be known. τ_R is the mean time between molecular reorientations.[33] The relationship between the correlation time τ_R and the relaxation times (T_1, $T_{1\rho H}$, etc.) is given by the correlation time curve (Figure 1).[33,36,41] For temperature dependent relaxation time measurements two cases have to be distinguished. In the slow motion regime of the correlation time curve increasing temperatures correspond with decreasing relaxation times. However, in the fast motion regime the relaxation times increase with rising temperature. Therefore, temperature dependent measurements of the appropriate relaxation time (in most cases this will be $T_{1\rho H}$ or T_2) are a necessity, in order to compare the mobilities of different polymers on a qualitative basis.

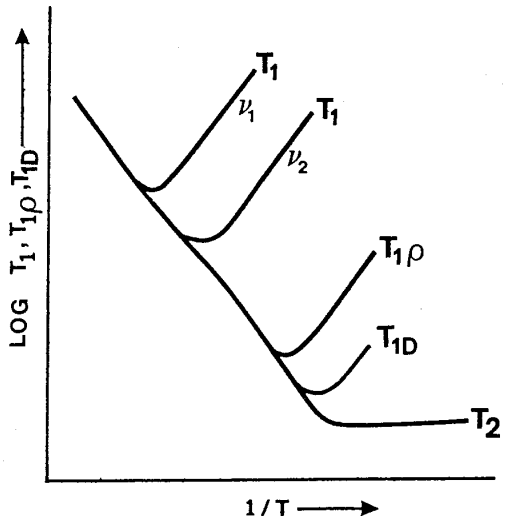

Figure 1. General behavior of relaxation times as functions of temperature. T_1 is the longitudinal or spin lattice relaxation time, T_2 is the transversal or spin spin relaxation time, T_{1D} is the T_1 relaxation in the dipolar field H_D (ν_1 and ν_2 are different spectrometer frequencies: the lower the spectrometer frequency the more the minimum of the T_1 curve (or of any other relaxation time curve) shifts to lower temperatures).[33]

Another parameter which reflects the mobility of a given compound is the cross–polarization constant T_{XH} for the heteronuclei X being under investigation.[36] Figure 2 demonstrates schematically the evolution of a signal of a heteronucleus in a cross–

polarization NMR experiment in dependence on the contact time. The signal increase is determined by T_{XH} – which expresses equally the magnetization speed – while the signal decrease is determined by $T_{1\rho H}$. The cross–polarization constant T_{XH} is determined in the so called 'variable contact–time experiment'.[42] The quality and the speed of the magnetization transfer from the abundant proton spin system to the dilute heteronuclei spin system depends mainly on the amount of protons, their distance to the heteronuclei, and the mobility of the functional group containing the heteronucleus. An estimation of the mobility of two functional groups, therefore, is allowed only, if similar proton surroundings are present. With increasing mobility the magnetization transfer becomes slower, as a consequence of decreasing proton dipole–dipole interactions in the sample. Thus higher T_{XH} values are indicating a higher mobility.[43,44]

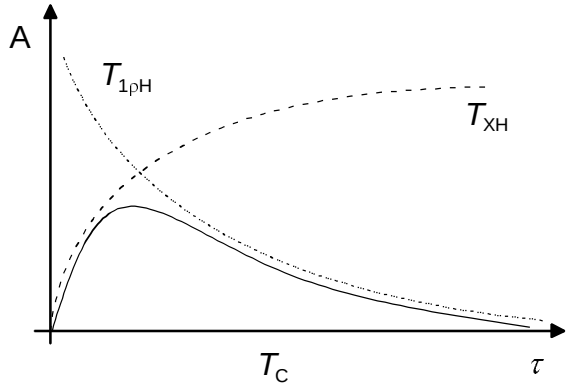

Figure 2. Schematic plot of signal intensity A versus time τ in a cross polarization (CP) NMR experiment.

In order to quantify the ^{29}Si NMR spectra, the real signal intensities of the siloxane subspecies of the investigated polymers (D^0 – D^2, T^0 – T^3, and Q^1 – Q^4)[17] must be calculated by eq. (2). The parameters $T_{1\rho H}$, T_{SiH}, and the signal intensities in dependence of the contact time $I(T_C)$ have to be determined first by the above–mentioned dynamic NMR experiments.[42]

$$I(T_C) = \frac{I_0}{\left(1 - T_{SiH}/T_{1\rho H}\right)}\left(e^{-T_C/T_{1\rho H}} - e^{-T_C/T_{SiH}}\right) \qquad (2)$$

In a subsequent step the degrees of condensation of the different silyl–functionalities D, T, and Q are calculated.[7,18,45]

2.1.2.2. Suspended State NMR Spectroscopy

NMR spectroscopy in interphases, which means a suspended state, gains increasing interest, because of the possibility to record spectra in a 'real' interphase. If sufficient swelling abilities of the polymers are assumed it is possible to record ^{1}H NMR spectra with very good resolution, which, in the best cases, reaches the resolution of spectra recorded in homogenous solutions.[46]

The necessary equipment to record NMR spectra in the suspended state is the same that is used for recording solid state NMR spectra (see Experimental Section). ^{1}H high resolution MAS spectra are recorded with a simple single pulse excitation sequence and medium fast magic angle spinning frequencies (~ 4000 Hz). By suspending the polymers in any kind of solvent that induces swelling the dipole–dipole interactions between the protons in the polymers are largely reduced. As a consequence the relaxation mechanisms are no longer controlled by spin–diffusion; this means on the one hand that resolved spectra with narrow line widths can be recorded, and on the other hand that for different proton sites in the polymers different relaxation rates can be expected. Since swelling of inorganic–organic hybrid polymers is less distinct compared to pure organic polymers, week proton dipole–dipole interactions are always present. This can be utilized to perform CP/MAS NMR experiments on interphases in order to record signals of ^{13}C, or ^{31}P sites. The advantage of CP/MAS over single pulse HPDEC NMR experiments in this special case is that signals of heteronuclei of the employed solvent are not recorded because of the lack of a magnetization transfer to the nuclear spins of these solvent molecules.

2.1.2.3. Dynamic Deuterium NMR Spectroscopy

^{2}H NMR spectroscopy is a well-established technique for the evaluation of molecular motions in various types of solids. The deuterium nucleus has a spin of 1 along with a finite nuclear quadrupole moment. The interaction of the quadrupole moment with the electric field gradient of the surrounding electrons gives rise to a perturbation of the Zeeman levels which results in two transitions of different energies. In the rigid limit case, i.e. in the absence of any molecular motion, the corresponding transition frequencies are given by[47–49]

$$n = n_0 \pm \frac{3}{8}\frac{e^2 qQ}{h}\left(3\cos^2 q\text{-}1\text{-}h\sin^2 q\cos 2j\right) \quad (3)$$

e^2qQ/h and η are designated as quadrupolar coupling constant (typically 186 kHz for an aromatic C–D bond) and the asymmetry parameter, respectively. θ and φ are the Euler angles which define the orientation of the C–D bond direction with respect to the external magnetic field $\mathbf{B}_0$. In a polycrystalline (rigid) solid the summation over all orientations of the C–D bond direction results in a typical Pake pattern, as shown in Figure 3. The distance between the perpendicular singularities is approximately d = 138 kHz (d = ¾ e^2qQ/h). Molecular motions with rate constants higher than 10^3 s^{-1} are accompanied by distinct lineshape changes which reflect directly the type and time–scale of the underlying motion(s). For instance, a 180^o flip of a deuterated phenyl ring gives rise to a characteristic 'fast-exchange limit' ^{2}H NMR spectrum (with $k \geq 10^8$ s^{-1}), as demonstrated in Figure 3.

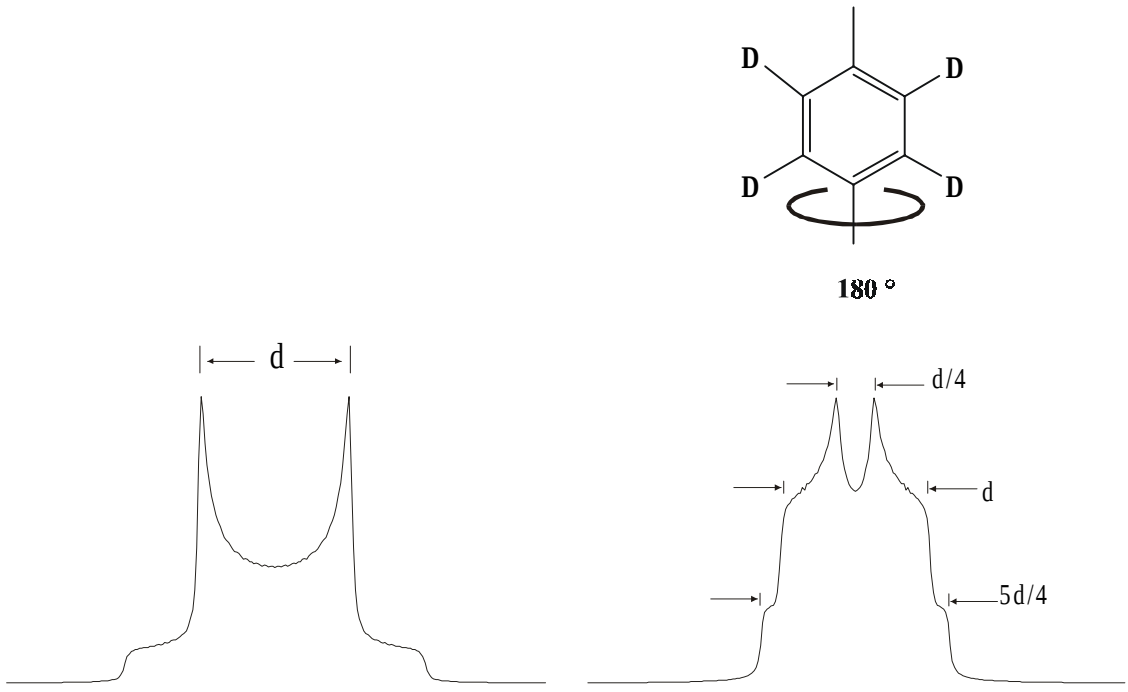

Figure 3. Typical lineshapes for a static sample (left) and 180° phenyl ring flips (right).

2.1.2.4. Computational Methods

To analyze and visualize the NMR data set comprised in Table 2, a program (kd2) written in C was employed, implementing the well–known self–organizing feature map of Kohonen. The NMR data were saved as ASCII and some standard data preprocessing techniques were applied – standardizing and scaling. Some of the parameters reveal larger values than others and it was assured, that this did not affect the evaluation – all parameters had to be treated equally. Therefore, the mean and standard deviation of all parameters were computed. The corresponding mean was subtracted from each value and the result was divided by the standard deviation subsequently. After standardization each parameter had a mean of zero and a standard deviation of one. For further processing, all values were scaled to the desired input range of the neural network.

These data were read by 'kd2' and used to train the self–organizing feature map. Despite the term “self–organizing”, some parameters have to be supplied to the program. The most important parameter is the size of the desired map. For classification purposes

there are some rules of thumb on how big (or small) the map should be. If the map is used for visualization only, much larger maps have to be employed. Smaller maps can be applied to verify the results afterwards. Other possible parameters include the adaptation function, adaptation height and adaptation width at the beginning and at the end of the training and the number of training cycles. For each of these parameters standard parameters can be used. Best results are obtained, if the adaptation height and adaptation width are decreased exponentially during the training.[50] The resulting map is saved as ASCII and then visualized by other programs. To analyze the quality of the maps, the programs 'pks' and 'winnerdist' were utilized to produce component–maps, u–matrix–maps, and distance–maps. Regarding these derived maps, statements are possible whether any folding or defects are present and how well the compounds are distributed or separated on the map.

In order to better visualize the inherent structures of the Kohonen maps the big and the small map, each, have been combined with the corresponding distance–maps (Figures 25 and 28, chapter 3.2.). These distance–maps are derived of the Euclidean distances between all the neurons on the Kohonen map. Each compound on this map is described by ten parameters (Table 2). This can be regarded as a vector in a ten-dimensional data space where similar compounds are found close to each other. To visualize the neighborhoods and distribution in this data space, a mapping is required that projects the data on a two–dimensional plane while preserving the neighborhood relationships. The Kohonen Self Organizing Feature Map provides such a nonlinear and topology–preserving mapping. Each position (neuron) on that two–dimensional map is associated with a weight vector (also called codebook–vector) and represents a region in the data space. Neurons that have the same distances on the map can have different distances in the data space. To visualize this fact, gray levels are introduced between each two neighboring neurons on the map. These gray levels correspond to the distances of the neurons in the data space. Usually

these distances are measured by the Euclidean distances. Therefore, not only information about neighborhoods (similarities) in the data space, but also about the distances can be visualized.

To have a closer look on the distances a similar method is the so–called u–matrix (Unified Matrix).[51] If, for every neuron of the SOM, the distances to the eight immediate neighbors are summed up, a measure of dissimilarity between neurons in the ten–dimensional data space is obtained. This sum of distances for every neuron can be displayed by different gray levels and expressed as the u-matrix. Black neurons on the u-matrix represent large distances or borders between regions in the data space, while white neurons represent regions where neurons are located close to each other in the data space.

To justify the use of neural networks the results were compared with the most common data evaluation method – the *p*rinciple *c*omponent *a*nalysis (pca). These evaluations have been made using the commercially available product 'SPSS' with the same preprocessed data as input.

Table 1. Inorganic–organic hybrid polymers

entry	chemical structure	ideal stoichio-metry	ref.
1	ligand **A:** 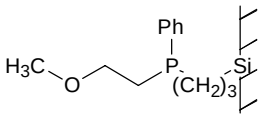 co-condensed with $Si(OCH_3)_4$	**T:Q = 1:2**	7
2	ligand **B:** 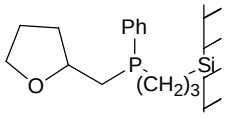 co-condensed with $Si(OCH_3)_4$	**T:Q = 1:2**	7
3	ligand **C:** 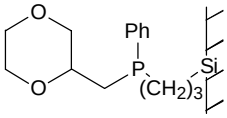 co-condensed with $Si(OCH_3)_4$	**T:Q = 1:2**	7
4	complex **I**: 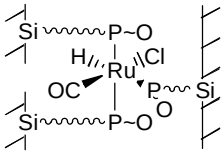 with ligand **A** co-condensed with $Si(OCH_3)_4$	**T:Q = 1:6**	7
5	complex **I** with ligand: **B**, co-condensed with $Si(OCH_3)_4$	**T:Q = 1:6**	7
6	complex **I** with ligand **C**, co-condensed with $Si(OCH_3)_4$	**T:Q = 1:6**	7
7	ligand **A**: 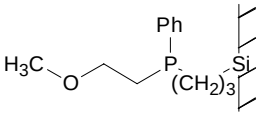 co-condensed with $(H_3C)_2Si(OCH_3)_2$	**T:D = 1:1.5**	15
8	ligand **D**: 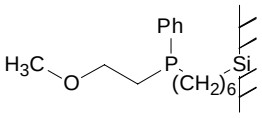 co-condensed with $(H_3C)_2Si(OCH_3)_2$	**T:D = 1:1.1**	15
9	ligand **E**: 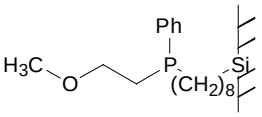 co-condensed with $(H_3C)_2Si(OCH_3)_2$	**T:D = 1:1.4**	15
10	ligand **A** co-condensed with $(H_3C)Si(OCH_3)_3$	**T:T = 1:2**	15
11	ligand **D** co-condensed with $(H_3C)Si(OCH_3)_3$	**T:T = 1:2**	15
12	ligand **E** co-condensed with $(H_3C)Si(OCH_3)_3$	**T:T = 1:2**	15

Table 1. Continuation

13	ligand **A** co-condensed with $Si(OCH_3)_4$	**T:Q = 1:2**	15
14	ligand **D** co-condensed with $Si(OCH_3)_4$	**T:Q = 1:2**	15
15	ligand **E** co-condensed with $Si(OCH_3)_4$	**T:Q = 1:2**	15
16	complex **I** with ligand **A** co-condensed with $(H_3C)_2Si(OCH_3)_2$	**T:D = 3:4.6**	15
17	complex **I** with ligand **D** co-condensed with $(H_3C)_2Si(OCH_3)_2$	**T:D = 3:3.3**	15
18	complex **I** with ligand **E** co-condensed with $(H_3C)_2Si(OCH_3)_2$	**T:D = 3:1.5**	15
19	complex **I** with ligand **A** co-condensed with $(H_3C)Si(OCH_3)_3$	**T:T = 1:2**	15
20	complex **I** with ligand **D** co-condensed with $(H_3C)Si(OCH_3)_3$	**T:T = 1:2**	15
21	complex **I** with ligand **E** co-condensed with $(H_3C)Si(OCH_3)_3$	**T:T = 1:2**	15
22	complex **I** with ligand **A** co-condensed with $Si(OCH_3)_4$	**T:Q = 1:2**	15
23	complex **I** with ligand **D** co-condensed with $Si(OCH_3)_4$	**T:Q = 1:2**	15
24	complex **I** with ligand **E** co-condensed with $Si(OCH_3)_4$	**T:Q = 1:2**	15
25	ligand **A** co-condensed with co-condensing agent **a**: 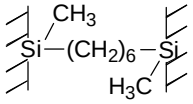	**T:D = 1:1**	18
26	ligand **A** co-condensed with co-condensing agent **b**: 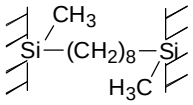	**T:D = 1:1**	18
27	ligand **A** co-condensed with co-condensing agent **c**: 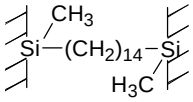	**T:D = 1:1**	18
28	complex **II**: 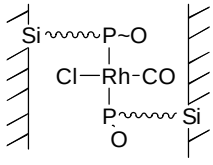 with ligand **A** co-condensed with co-condensing agent **a**	**T:D = 2:1**	18
29	complex **II** co-condensed with co-condensing agent **a**	**T:D = 1:1**	18
30	complex **II** co-condensed with co-condensing agent **a**	**T:D = 1:2**	18
31	complex **II** co-condensed with co-condensing agent **a**	**T:D = 1:4**	18
32	complex **II** co-condensed with co-condensing agent **a**	**T:D = 1:8**	18
33	complex **II** co-condensed with co-condensing agent **a**	**T:D = 1:16**	18
34	complex **II** co-condensed with co-condensing agent **b**	**T:D = 1:1**	18
35	complex **II** co-condensed with co-condensing agent **c**	**T:D = 1:1**	18

Table 1. Continuation

36	ligand **F**: 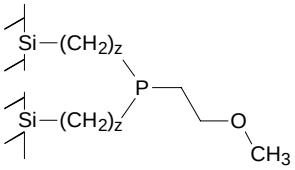 co-condensed with co-condensing agent a, z = 3	**T:D = 2:1**	22
37	ligand **G**: 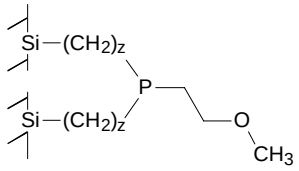 co-condensed with co-condensing agent **a**, z = 6	**T:D = 2:1**	22
38	ligand **G** co-condensed with co-condensing agent **a**, z = 6	**T:D = 1:1**	22
39	ligand **G** co-condensed with co-condensing agent **a**, z = 6	**T:D = 1:2**	22
40	ligand **H**: 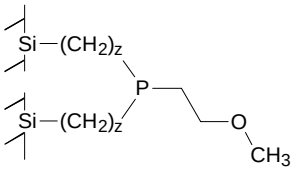 co-condensed with co-condensing agent **a**, z = 8	**T:D = 2:1**	22
41	ligand **K**: 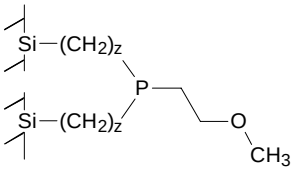 co-condensed with co-condensing agent **a**, z = 14	**T:D = 2:1**	22
42	complex **III**: 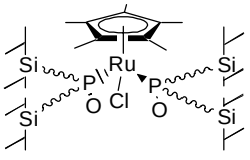 with ligand **F** co-condensed with co-condensing agent **a**	**T:D = 4:1**	22
43	complex **III** with ligand **G** co-condensed with co condensing-agent **a**	**T:D = 4:1**	22
44	complex **III** with ligand **H** co-condensed with co condensing-agent **a**	**T:D = 4:1**	22
45	complex **IV**: 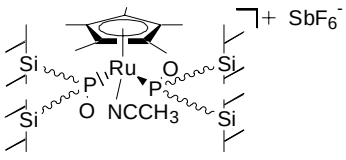 with ligand **G** co-condensed with co-condensing agent **a**	**T:D = 1:1**	22

Table 1. Continuation

46	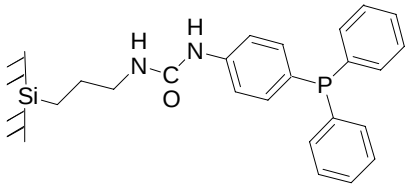 ligand **L**: co-condensed with co-condensing agent **a**	**T:D = 1:5**	52
47	ligand **L** co-condensed with co-condensing agent **d**: 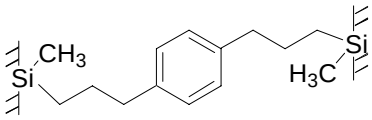	**T:D = 1:5**	52
48	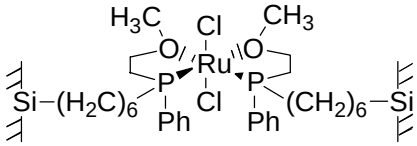 complex **VI**: co-condensed with co-condensing agent **d**	**T:D = 1:6**	52
49	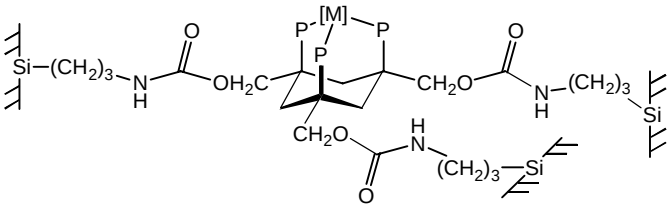 complex **VII**: co-condensed with itself, [M] = $Mo(CO)_3$	**T:Q = 1:0**	53
50	complex **VII** co-condensed with $Si(OCH_3)_4$	**T:Q = 1:1**	53
51	complex **VII** co-condensed with $Si(OCH_3)_4$	**T:Q = 1:4**	53
52	complex **VIII**: 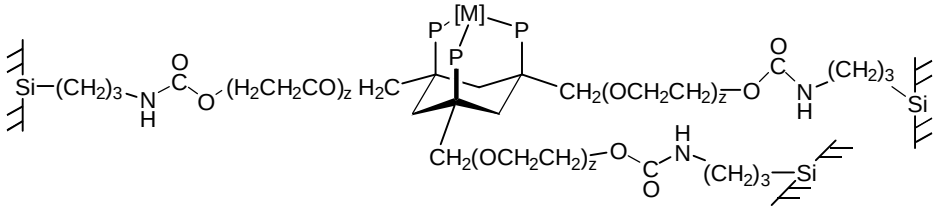 co-condensed with itself, [M] = $Mo(CO)_3$; z = 9	**T:Q = 1:0**	53
53	complex **VIII** (z = 9) co-condensed with $Si(OCH_3)_4$	**T:Q = 1:1**	53
54	complex **VIII** (z = 9) co-condensed with $Si(OCH_3)_4$	**T:Q = 1:4**	53
55	complex **VIII** (z = 120) co-condensed with itself	**T:Q = 1:0**	53
56	complex **VIII** (z = 120) co-condensed with $Si(OCH_3)_4$	**T:Q = 1:1**	53
57	complex **VIII** (z = 120) co-condensed with $Si(OCH_3)_4$	**T:Q = 1:4**	53
58	complex **VIII** (z = 230) co-condensed with itself	**T:Q = 1:0**	53
59	complex **VIII** (z = 230) co-condensed with $Si(OCH_3)_4$	**T:Q = 1:1**	53
60	complex **VIII** (z = 230) co-condensed with $Si(OCH_3)_4$	**T:Q = 1:4**	53

Table 1. Continuation

61	complex **VIII** (z = 270) co-condensed with itself	**T:Q = 1:0**	53
62	complex **VIII** (z = 270) co-condensed with $Si(OCH_3)_4$	**T:Q = 1:1**	53
63	complex **VIII** (z = 270) co-condensed with $Si(OCH_3)_4$	**T:Q = 1:4**	53
64	complex **IX**: 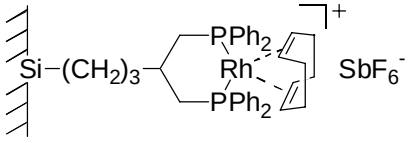 co-condensed with co-condensing agent **d**	**T:D = 1:20**	54
65	complex **X**: 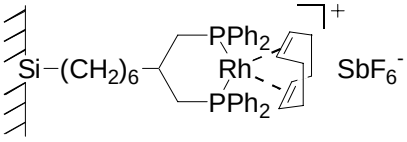 co-condensed with itself	**T:D = 1:0**	54
66	complex **X** co-condensed with co-condensing agent **a**	**T:D = 1:5**	54
67	complex **X** co-condensed with co-condensing agent **a**	**T:D = 1:20**	54
68	complex **X** co-condensed with co-condensing agent **d**	**T:D = 1:5**	54
69	complex **X** co-condensed with co-condensing agent **d**	**T:D = 1:20**	54
70	ligand **L**: 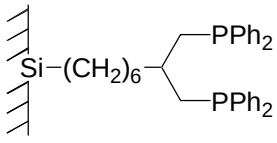 co-condensed with co-condensing agent **d**	**T:D = 1:5**	54
71	ligand **L** co-condensed with co-condensing agent **d**	**T:D = 1:10**	54
72	ligand **L** co-condensed with co-condensing agent **a**	**T:D = 1:10**	54
73	co-condensing agent **d**: 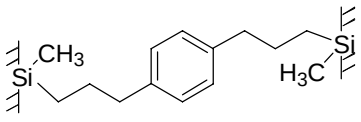	**D:D = 1:1**	23
74	co-condensing agent **e**: 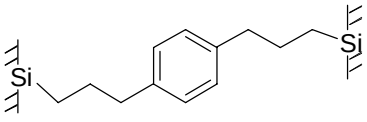	**T:T = 1:1**	23
75	co-condensing agent **f**: 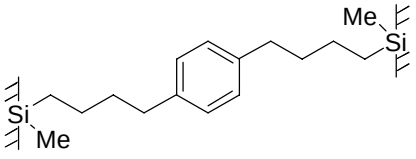	**D:D = 1:1**	23
76	co-condensing agent **d** co-condensed with $(H_3C)Si(OCH_3)_3$	**D:T = 4:1**	23
77	co-condensing agent **e** co-condensed with $(H_3C)Si(OCH_3)_3$	**T:T = 4:1**	23
78	co-condensing agent **f** co-condensed with $(H_3C)Si(OCH_3)_3$	**D:T = 8:1**	23
79	co-condensing agent **d** co-condensed with co-condensing agent **e**	**D:T = 1:1**	23

Table 1. Continuation

80	co-condensing agent **g**: 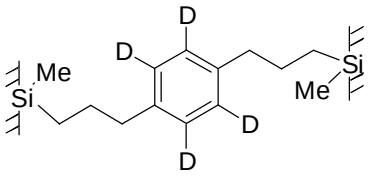 sol-gel processed in MeOH	**D:D = 1:1**	55
81	co-condensing agent **g** sol-gel processed in THF	**D:D = 1:1**	55
82	co-condensing agent **h**: 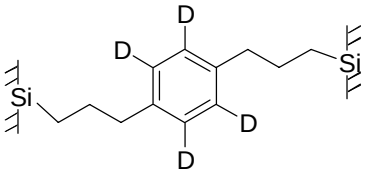 sol-gel processed in MeOH	**T:T = 1:1**	55
83	co-condensing agent **h** sol-gel processed in THF	**T:T = 1:1**	55
84	co-condensing agent **g**: 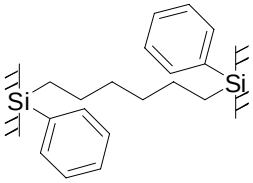	**D:D = 1:1**	52

Table 2. NMR Data of the compounds evaluated by the SOM

entry	T_{PH}	$T_{1\rho H}$ (P) [a]	$T_{1\rho H}$ (Si) [b]	**T^0** [c]	**T^1** [c]	**T^2** [c]	**T^3** [c]	**D** [d]	**T** [d]	**Q** [d]	type [e]
1	0.58	2.9	2.5			21.8	93.1		94.0	84.0	***Q***
2	0.23	4.4	3.7			25.9	66.7		91.0	82.0	***Q***
3	0.24	4.9	4.0			24.7	87.6		93.0	84.0	***Q***
4	0.22	5.8	5.5			32.3	68.8		86.0	83.0	***Q***
5	0.17	6.1	5.4			33.0	68.1		86.0	83.0	***Q***
6	0.18	6.2	5.4			32.3	61.5		83.0	81.0	***Q***
7	2.01	6.9	3.6			20.1	51.8	96.0	91.0		***D***
8	1.79	3.6	4.3			27.0	73.0	98.0	91.0		***D***
9	2.15	7.2	5.1				71.4	100.0	100.0		***D***
10	0.36	1.6	2.2		4.0	29.3	100.0		91.0		***T***
11	0.56	1.1	2.9			28.2	100.0		93.0		***T***
12	0.71	2.0	2.3			25.0	100.0		93.0		***T***
13	0.29	1.4	2.5			21.8	93.1		94.0	84.0	***Q***
14	0.32	1.4	1.6			25.7	69.5		91.0	86.0	***Q***
15	0.52	1.4	3.4			56.8	48.4		82.0	78.0	***Q***
16	0.22	3.8	6.0		2.4	37.4	41.4	88.0	83.0		***D***
17	0.2	4.3	5.1		7.5	56.7	85.1	82.0	84.0		***D***
18	0.23	4.5	5.1		16.7	100.0	91.7	80.0	78.0		***D***
19	0.2	2.8	5.2		19.6	58.9	100.0		82.0		***T***
20	0.21	5.6	5.4		3.2	58.1	100.0		87.0		***T***
21	0.20	4.1	5.2		7.4	77.8	100.0		83.0		***T***
22	0.23	2.6	5.5		6.5	32.3	68.8		86.0	83.0	***Q***
23	0.20	4.8	5.3		2.5	67.9	53.1		80.0	83.0	***Q***
24	0.20	4.9	5.0			39.7	36.6		83.0	80.0	***Q***
25	0.64	2.0	2.1			15.5	44.3	88.0	91.0		***D***
26	0.56	2.1	2.5			13.8	40.4	93.0	92.0		***D***
27	0.91	2.1	2.0			22.6	36.1	96.0	87.0		***D***
28	0.26	4.7	6.5		29.2	99.0	100.0	75.0	77.0		***D***
29	0.22	5.4	5.5		6.5	30.9	45.1	73.0	82.0		***D***
30	0.27	5.1	6.7			9.2	23.9	83.0	91.0		***D***
31	0.27	4.8	6.5			4.5	11.7	82.0	91.0		***D***
32	0.25	5.6	8.8			2.2	4.9	86.0	90.0		***D***
33	0.27	4.0	5.8			1.1	3.1	86.0	91.0		***D***
34	0.23	4.3	4.9		3.9	36.3	42.1	76.0	82.0		***D***
35	0.25	2.7	4.8		0.1	31.3	37.2	85.0	85.0		***D***
36	0.26	7.8	7.1			33.3	46.3	90.2	87.3		***D***
37	0.36	10.0	6.8			38.9	56.3	91.4	86.4		***D***
38	0.41	9.8	10.9			10.1	27.6	95.7	91.0		***D***
39	0.41	8.9	14.6			6.4	17.3	96.8	91.4		***D***
40	1.36	2.0	5.4			48.7	68.0	93.0	86.1		***D***
41	1.23	3.4	8.1			31.9	43.1	96.0	85.1		***D***
42	0.15	5.2	6.6		55.6	100.0	51.0	52.1	65.9		***D***
43	0.16	6.6	6.3		35.6	100.0	91.0	56.2	74.8		***D***
44	0.15	5.4	5.2		50.5	100.0	85.1	78.0	71.6		***D***
45	0.22	11.1	9.4			25.8	38.1	96.0	85.8		***D***
46	2.05	8.3	7.1			6.1	20.8	91.5	92.6		***D***
47	1.94	6.5	6.8			2.6	18.7	91.7	95.9		***D***

Table 2. Continuation

48	0.39	7.8	7.8			7.8	10.1	98.6	85.5		***D***
49	0.54	5.8	5.5	48.0	92.9	100.0	41.5		49.3		***T***
50	0.45	6.9	5.3	21.0	44.2	47.7	2.1		42.3	94.8	***Q***
51	0.63	6.5	4.9	7.1	15.6	15.7	2.0		43.5	88.6	***Q***
52	0.95	5.1	2.6	9.8	39.4	59.2	100.0		73.0		***T***
53	0.43	6.9	2.3	8.9	39.4	61.4	84.1		71.4	83.7	***Q***
54	0.69	6.6	2.2	2.0	10.2	13.1	15.1		67.4	85.9	***Q***
55	0.48	1.2	2.5		2.9	37.3	100.0		89.9		***T***
56	0.48	1.4	2.0		3.9	51.1	100.0		87.3	88.5	***Q***
57	0.55	1.5	1.8		1.0	14.2	28.0		87.4	90.1	***Q***
58	0.37	1.3	1.6				100.0		100.0		***T***
59	0.53	1.9	1.5			7.4	100.0		97.7	89.6	***Q***
60	0.49	2.0	1.5			3.2	37.2		100.0	93.1	***Q***
61	0.75	1.4	1.6				100.0		100.0		***T***
62	0.64	1.9	1.6				100.0		100.0	89.8	***Q***
63	0.74	1.7	1.5			2.6	30.7		97.4	91.0	***Q***
64	0.74	7.6	5.6			13.3	4.3	83.3	75.1		***D***
65	0.20	15.0	13.7			93.1	100.0		83.8		***T***
66	0.93	12.0	12.7			12.5	9.8	85.5	81.5		***D***
67	0.65	10.2	8.0			2.9	7.7	76.1	90.9		***D***
68	0.61	10.1	11.8			19.7	17.7	89.4	82.4		***D***
69	0.26	6.8	3.3				6.6	100.0	100.0		***D***
70	0.42	0.6	1.4			11.2	26.6	90.0	88.0		***D***
71	0.41	1.73	2.6			13.4	14.2	84.0	81.0		***D***
72	0.32	0.46	2.3			2.1	9.4	88.0	94.0		***D***

[a] Determined via ^{31}P CP/MAS NMR experiments. [b] Determined via ^{29}Si CP/MAS NMR experiments. [c] **T^0 – T^1**: silyl subspecies, see ref.[17,20] [d] **D**, **T**, **Q**: degrees of condensation of the corresponding silyl species. [e] ***D***, ***T***, ***Q***: D type, T type, or Q type co–condensing agent based polymers.

3. General Section – Discussion

3.1. Mobility Studies on Inorganic–Organic Hybrid Polymers

3.1.1. ^{29}Si CP/MAS NMR Spectroscopy

Most of the polymers listed in Table 1 (entries **1** – **45** and **49** – **72**) have been synthesized by other members of the group and were thoroughly characterized earlier.[7,15,18,22,53,54] Their NMR relaxation data are subject of the evaluation with a neural network (see chapter 3.2).

The analysis of the ^{29}Si CP/MAS spectra and the corresponding relaxation time measurements (T_{SiH}, $T_{1\rho H}$) confirm the homogeneity of the inorganic–organic hybrid polymers **46** – **48** and **73** – **84** (Table 1). In each case only one value for $T_{1\rho H}$ could be determined, which is in agreement with earlier findings.[7,15,18]

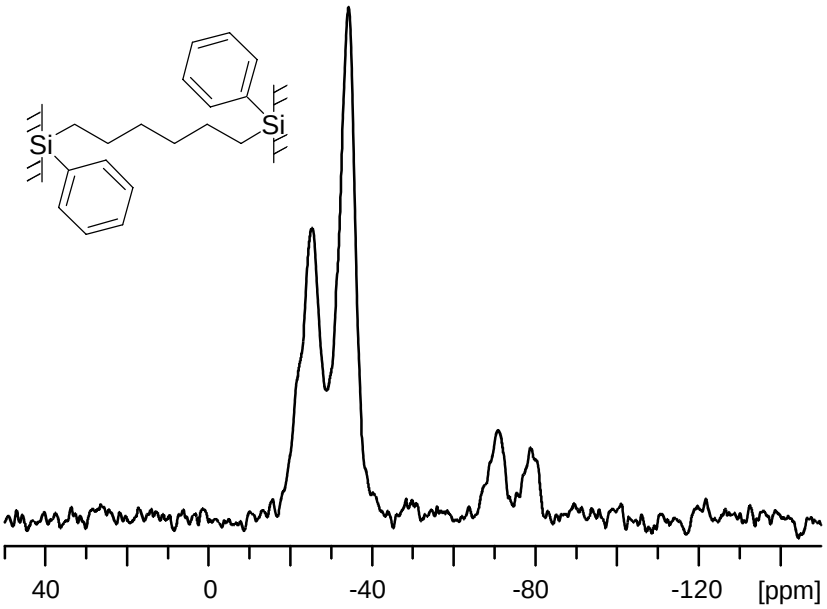

Figure 4. ^{29}Si CP/MAS NMR spectrum of compound **84**. Assignment of signals see text.

The chemical shift values at - 25.4 and - 34.3 ppm correspond to D group signals of compound **84** (D^1 and D^2), the signals at - 71.1 and - 79.0 to T group signals of sol–gel processed $PhSiHCl_2$ (T^2 and T^3) which is one of the educts of **84**. The signals of the silyl

species in the spectrum of compound **84** are shifted to higher field because of the phenyl group attached to the silicon atom (Figure 4). In Table 3 the relative intensities of the signals of the silyl subspecies, degrees of condensation, and if appropriate the degrees of hydrolysis of the polymers **46** – **48** and **73** – **84** are listed.

Compounds **46** and **47** show high degrees of condensation for both the D and the T type silyl species. In each case the solvent employed for the sol–gel process was THF. Despite different co–condensing agents the degrees of condensation and the signals in the ^{29}Si CP/MAS NMR spectra of **46** and **47** resemble each other very much. There seems to be no differences concerning the kinetics in sol–gel processing of $\mathbf{D^0–(CH_2)_6–D^0}$ or $\mathbf{D^0–(CH_2)_3–C_6H_4–(CH_2)_3–D^0}$ with functionalized silanes Fn–**T**. As a consequence the properties of the materials behave in an equal manner (see also the results of the dynamic NMR measurements).

Table 3. Relative I_0 data, degrees of condensation and degrees of hydrolysis of the silyl groups of polymers **46** – **48** and **73** – **84**

compound	relative I_0 data						degree of condensation		real T/D ratio	degree of hydrolysis [%]
	D^0	D^1	D^2	T^1	T^2	T^3	D	T		
46	1.5	17.4	100		6.1	20.8	92	93	1:4.4	
47	2.0	16.1	100		2.6	18.7	92	96	1:5.5	
48		2.9	100		7.8	10.1	99	86	1:5.8	99
73	2.3[a)]	70.7[a)]	100[a)]				78			90
74				37.3[a)]	100[a)]	36.3[a)]		67		78
75	5.6[a)]	45.8[a)]	100[a)]				81			90
76		67.1	100		12.4	21.9	80	88	1:3.7	99
77				19.4[a)]	100[a)]	35.6[a)]		70		
78	4.5[a)]	58.5[a)]	100[a)]		6.5[a)]	11.2[a)]	79	88	1:8.1	99
79		88.9	100	30.8	94.3	22.5	77	69	1:1.1	91
80		43.9	100				87			
81		19.8	100				92			
82				31.7	100	19.2		64		
83				29.4	100	16.6		64		
84		66,9	100				80			

[a)] Determined via ^{29}Si SPE/HPDEC Experiments.

As an example for the successful application of **73** as a co–condensing agent serves the sol–gel processed ruthenium complex **48**. The initial stoichiometry of T:D = 1:6 could be retained. The degrees of hydrolysis and condensation are very high, the solvent used in the sol–gel process was THF.

Compounds **73** – **79** have been sol–gel processed in MeOH and show low to medium degrees of condensation despite high degrees of hydrolysis (except **74**). Nevertheless, the initial stoichiometry of the polymers **76**, **78**, and **79** could be nearly retained after sol–gel processing, that means neither D nor T groups were washed out. This is a necessary prerequisite in order to successfully use the corresponding monomers as co–condensing agents in 'chemistry in interphases'.

The degrees of condensation determined for **80** and **81** differ in dependence on the solvent employed in sol–gel processing. Concerning D type co–condensing agents, THF leads to higher degrees of condensation (usually > 85%), while the utilization of MeOH results always in lower degrees of condensation (see also the other compounds listed in Table 3). There seems to be no influence of the solvent on the degrees of condensation of the T type materials **82** and **83**. Mixed D/T copolymers always show higher values of cross–linkage independent on the solvent applied for the sol–gel process.

Compound **84** is the most recent inorganic–organic hybrid polymer obtained by sol–gel processing of the co–condensing agent $[Ph(MeO)_2Si(CH_2)_6Si(OMe)_2Ph]$ synthesized by *T. Salesch*.[56] It is designed to increase the overall mobility of the polymers by combining the flexibility of an alkyl chain with phenyl groups attached to the silicon atoms in order to slightly reduce the cross-linkage by steric hindering. The material **84** shows a degree of condensation of 80% which is an average value for only D type polymers. Since the sol–gel process with $[Ph(MeO)_2Si(CH_2)_6Si(OMe)_2Ph]$ has been carried out only in MeOH it is impossible to relate this degree of condensation to the steric effect of the phenyl ring or the effective polarity of the silyl group. The sol–gel

process with this educt must be carried out at least in another solvent such as THF, to clarify this question.

The degrees of hydrolysis of the polymers **46** – **48** and **73** – **84** can be calculated only by evaluation of the signals of the residual non hydrolyzed methoxy or ethoxy groups in the ^{13}C NMR spectra.[57] For these calculations either the integration of HPDEC spectra with a sufficient number of scans (> 1500) or the evaluation of spectra of a series of contact time variation experiments can be applied.

3.1.2. ^{13}C and ^{31}P CP/MAS NMR Spectroscopy

^{13}C CP/MAS NMR spectroscopy is a very useful tool to examine the organic backbone of the polymer matrix. In the cases of compounds **46** – **48** and **73** – **84** the sol–gel processes had no influence on the structural integrity of the organic functions of these polymers. The ^{13}C chemical shift values determined for these polymers in the solid state correspond with the shifts recorded by high resolution solution NMR spectroscopy.[23,56] In Figures 5 – 7 the ^{13}C CP/MAS NMR spectra of selected stationary phases are depicted and the listings of the corresponding chemical shift values are given in Tables 4 – 6.

Despite the high degree of deuteration (> 80%) of **80** – **83** the magnetization transfer from the proton to the carbon spin system is sufficient in order to cross–polarize the aromatic carbon atoms. The signal intensities of the sites C6 and C7 did not suffer as it can be verified in Figure 6.

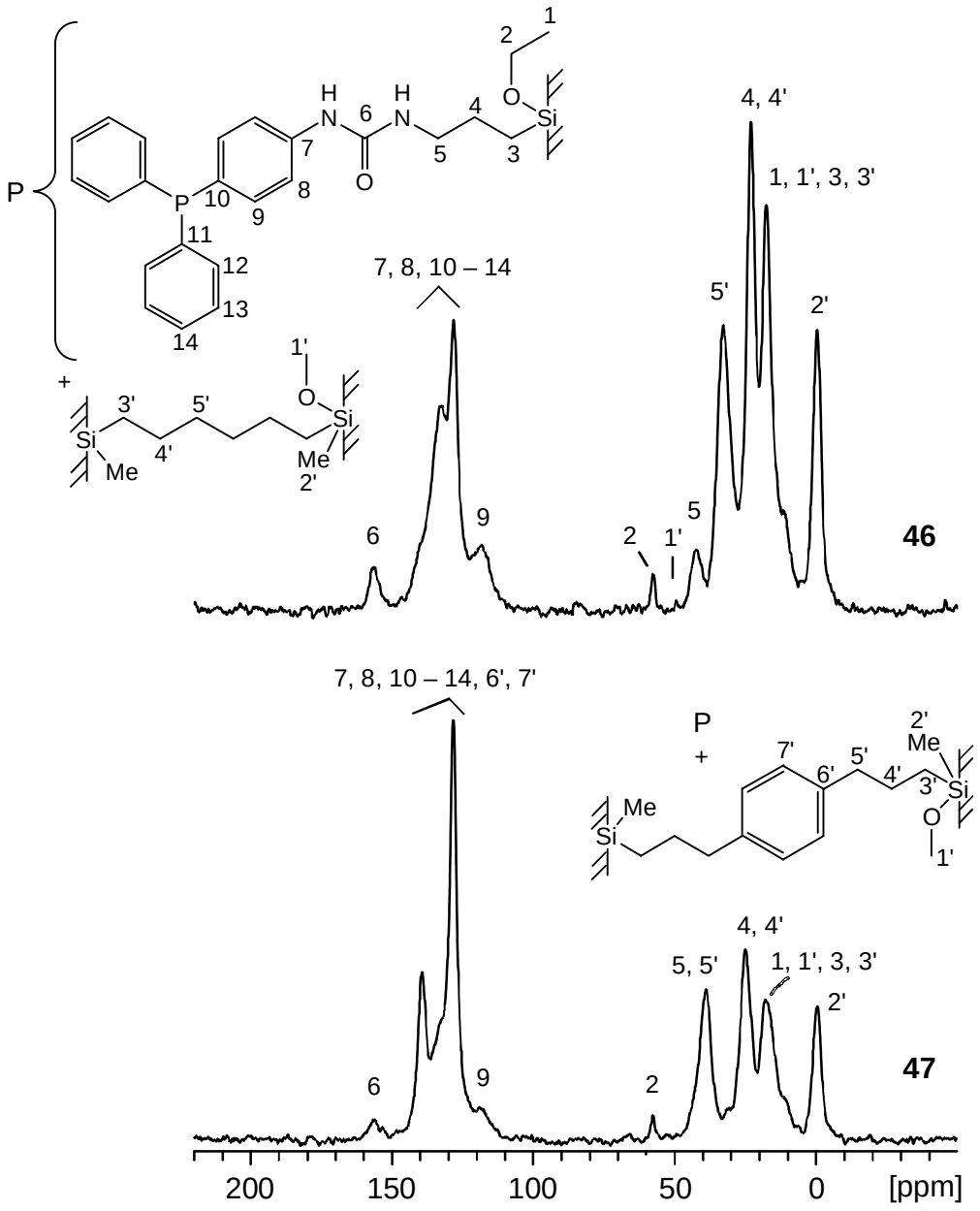

Figure 5. ^{13}C CP/MAS NMR spectra of compounds **46** and **47** (see also Table 4).

Table 4. ^{13}C chemical shift values of **46** and **47** [a)]

compound	δ ^{13}C [ppm]										
	C1, C1', C3, C3'	C2	C2'	C4, C4'	C5	C5'	C6	C6', C7	C7', C8, C12 – C14	C9	C10, C11
46	17.8	57.8	-0.3	23.1	42.3	33.0	156.7	139.0	133.2	118.5	128.4
47	17.8	57.7	-0.5	24.9	38.9	38.9	156.1	139.4	133.0	119.0	128.3

[a)] For labeling see Figure 5.

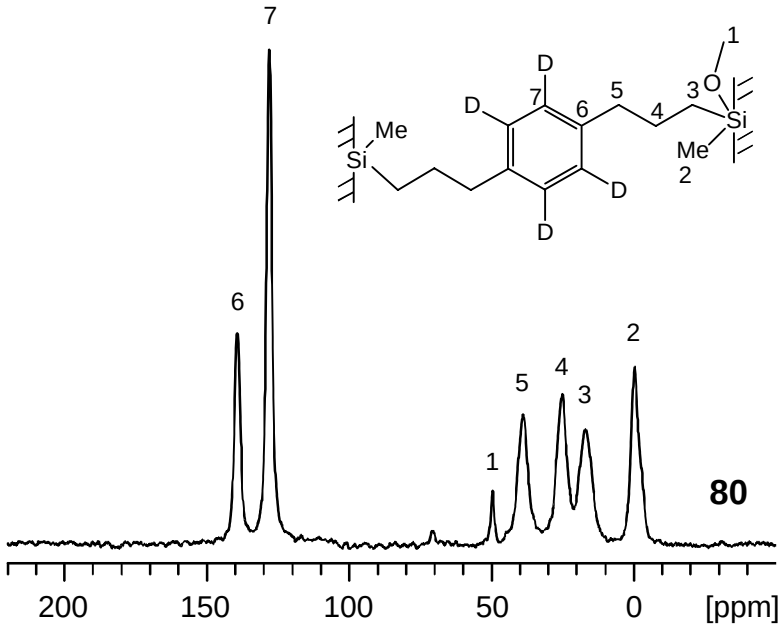

Figure 6. ^{13}C CP/MAS NMR spectrum of **80** (see also Table 5).

Table 5. ^{13}C chemical shift values of **80**

compound	δ ^{13}C [ppm]						
	C1	C2	C3	C4	C5	C6	C7
80	49.6	-0.3	17.0	25.2	38.9	139.3	128.1

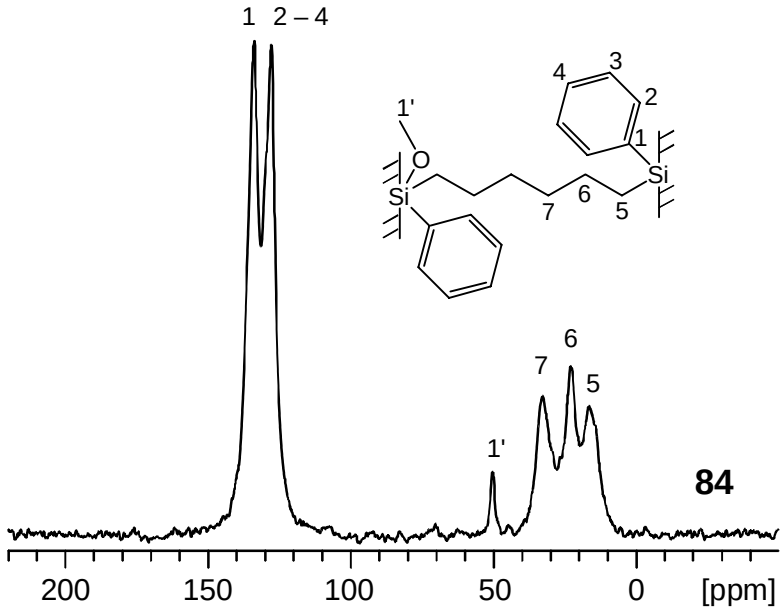

Figure 7. ^{13}C CP/MAS NMR spectrum of **84** (see also Table 6).

Table 6. ^{13}C chemical shift values of **84**

compound	δ ^{13}C [ppm]					
	C1	C1'	C2 – C4	C5	C6	C7
84	133.9	50.2	127.8	16.5	22.9	32.7

The ^{31}P CP/MAS NMR spectra of **46** and **47** resemble each other very much. The signals of the phosphorus atom are found at -6.3 ppm (**46**) and -6.7 ppm (**47**), respectively. The ^{31}P chemical shifts of these compounds are very close to that of triphenylphosphine (~ -5 ppm in solution), which means that the urea group which is located in the spacer of the phosphine ligand has no relevant electronic shielding effect on the phosphorus atom. This is an important finding, since these ligands were designed to transfer the properties of the soluble hydroformylation catalyst $H(CO)Rh(PPh_3)_3$ into the interphase. The evidence of the catalytic activity and selectivity of the corresponding 'interphase'–Rh complex has to be brought by future experiments.

3.1.3. Temperature Dependent $T_{1\rho H}$ Measurements

Multinuclear temperature dependent $T_{1\rho H}$ measurements in the solid state have been applied to compounds **46**, **47**, and **73** – **84**. This includes the detection of $T_{1\rho H}$ via ^{13}C, ^{29}Si, and ^{31}P CP/MAS NMR experiments which allows an estimation of the mobilities of different sites of the polymers. If the polymer being under investigation is built up homogeneously the values for $T_{1\rho H}$ detected for different functional sites (via ^{13}C, ^{29}Si, and ^{31}P) must be in the same order of magnitude.

The temperature dependence of $T_{1\rho H}$ of the polymers **73** – **76** in the dry state is depicted in Figure 8 (see also Table 7). The D type polymers **73** and **75** as well as the D/T mixed type polymer **76** reside in the slow motion regime of the correlation time curve. The T type compound **74** is just leaving the minimum of this curve tending to the left

side, nevertheless an assignment to the slow or the fast motion regime is not possible because of the only slight augmentation of $T_{1\rho H}$ in the observed temperature range.[36]

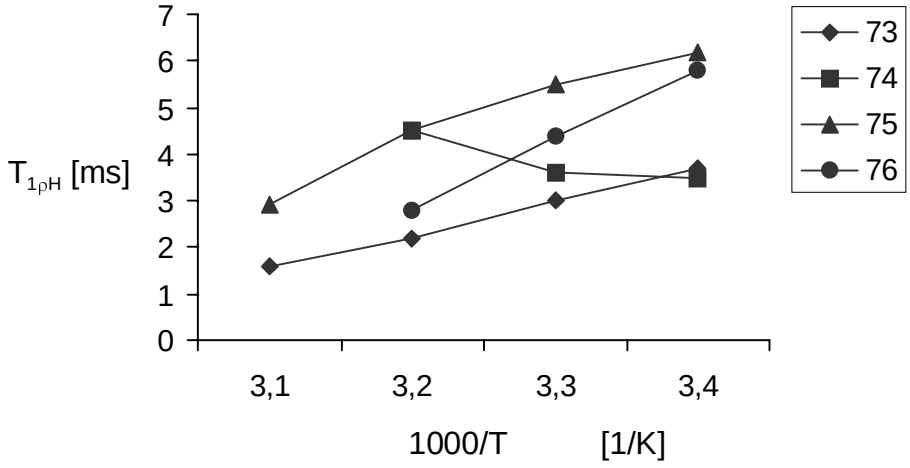

Figure 8. Temperature dependence of $T_{1\rho H}$ of **73** – **76** (see also Table 7).

A correlation of the temperature dependent $T_{1\rho H}$ values with the degrees of condensation, i.e. the cross–linkage is only possible for the D type polymers **73** and **75** and the mixed D/T copolymer **76**. Mobility seems to decrease in the order **73** > **76** > **75**, which is consistent with the increase of the relative cross-linkage of the D silyl species (**73**: 1.56, **76**: 1.6, **75**: 1.62).[58] At first sight it seems to be impossible to compare **74** with the former ones directly. Only the comparison of the T cross–linkage with the one determined for the mixed type copolymer **76** is consistent with the found mobilities (mobility: **74** > **76**, relative cross–linkage: 2.01, 2.64, respectively).

Table 7. Temperature dependent $T_{1\rho H}$ data of **73** – **76**

Compound	$T_{1\rho H}$ [ms] [a]				relative cross–linkage [c]	
	294 K	303 K	313 K	323 K	D	T
73	3.68	2.97	2.21	1.60	1.56	
74	3.45	3.60	4.48	[b]		2.01
75	6.15	5.49	4.46	2.88	1.62	
76	5.84	4.42	2.77	[b]	1.60	2.64

[a] Determined via ^{29}Si CP/MAS NMR experiments. [b] Not determined. [c] See ref.[58]

The behavior of compounds **80** – **83** is similar to the findings of compounds **73** and **74** (Figure 9 and Table 8). The D type polymers reside in the slow motion regime, while the T type polymers occupy the minimum of the correlation time curve. Since **80** and **81** as well as **82** and **83** are the deuterated derivatives of **73** and **74**, respectively, these results demonstrate that the sol–gel process is reproducible and measurements and evaluations of the relaxation times were set up correctly.

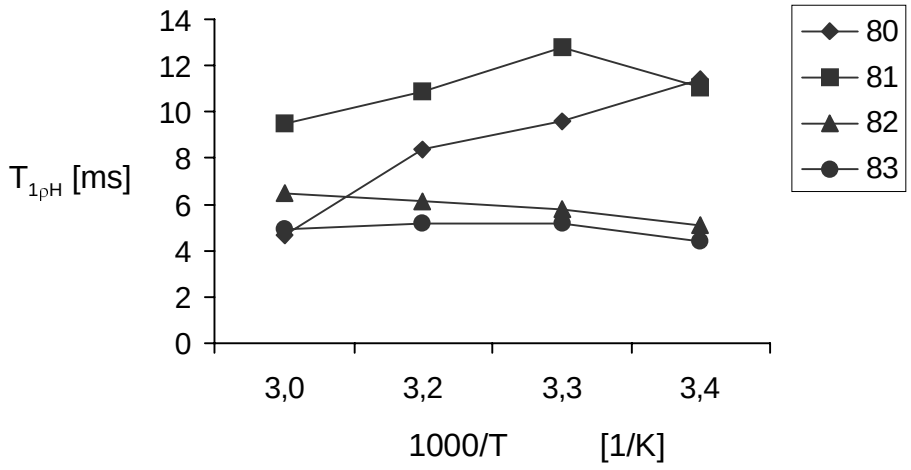

Figure 9. Temperature dependence of $T_{1\rho H}$ of **80** – **83** (see also Table 8).

Table 8. Temperature dependent $T_{1\rho H}$ data of **80** – **83**

Compound	$T_{1\rho H}$ [ms] [a]				relative cross–linkage	
	296 K	308 K	318 K	328 K	D	T
80	11.4	9.6	8.4	4.7	1.74	
81	11.1	12.8	10.9	9.5	1.84	
82	5.1	5.8	6.1	6.5		1.92
83	4.4	5.2	5.2	4.9		1.92

[a] Determined via ^{29}Si CP/MAS NMR experiments.

Compound **84** shows a lower relative cross–linkage than most of the other copolymers (**73**, **75**, **80**, and **81**) derived from D type co–condensing agents (Tables 7, 8, and 9). The strategy of using a steric demanding group such as a phenyl ring in order to reduce cross–linkage of the silyl species was successful. Polymer **84** resides in the slow

motion regime of the correlation time curve but is tending towards its minimum (Figure 10). Compared to the former materials **80** and **81** the stationary phase **84** seems to be more mobile in the dry state. As an example may serve the comparison of the ^{1}H SPE/MAS NMR spectra recorded of **73** (which is the non deuterated derivative of **80**) and **84** in the dry state under the same conditions (rot. freq. = 5000 Hz). The spectrum of **84** reveals a smaller spectral width than that one of **73** (Figure 11) which is in favor for the higher mobility of **84**.

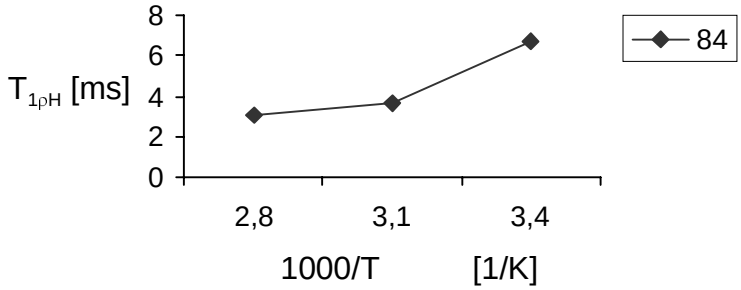

Figure 10. Temperature dependence of $T_{1\rho H}$ of **84** (see also Table 9).

Table 9. Temperature dependent $T_{1\rho H}$ data of **84**

Compound	$T_{1\rho H}$ [ms] [a)]			relative cross–linkage	
	294 K	320 K	355 K	D	T
84	6.7	3.7	3.1	1.6	

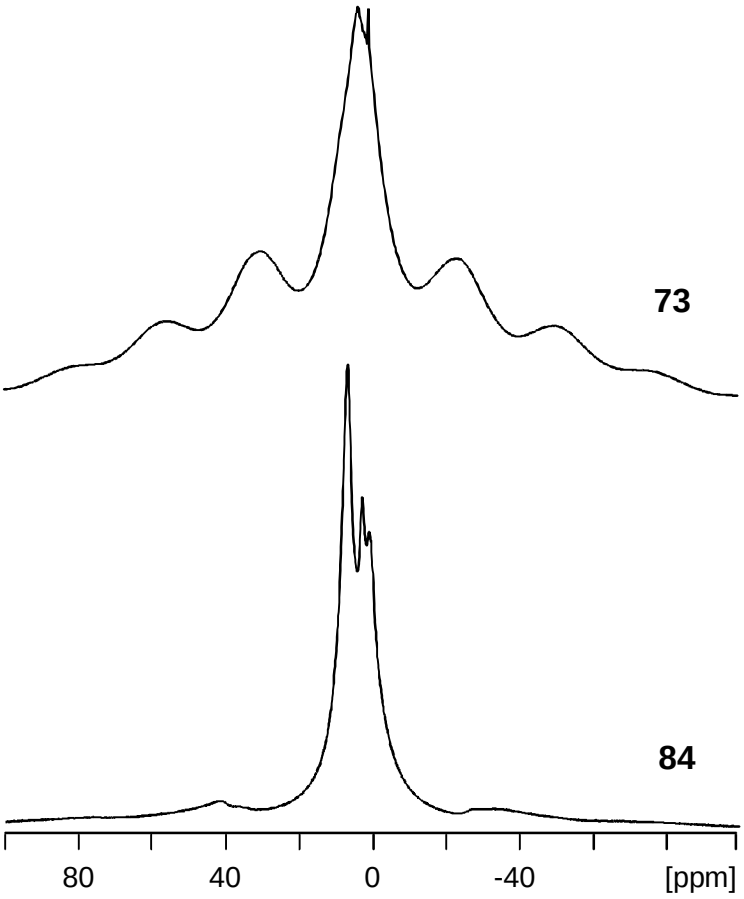

Figure 11. ^{1}H SPE/MAS NMR spectra of **73** and **84** recorded under the same conditions.

The determinations of $T_{1\rho H}$ of **46** and **47** (Figure 12 and Table 10) in the dry state have been carried out by ^{31}P CP/MAS NMR measurements, in order to monitor the mobilities of the phosphorus centers. According to the findings concerning the degrees of condensation (Table 3) both polymers show a very similar dynamic behavior. On a qualitative basis – by taking into account the slightly higher cross–linkage of the T groups of **47** and the higher values of $T_{1\rho H}$ of **46** – one can assume that **46** is somewhat more mobile than **47**.

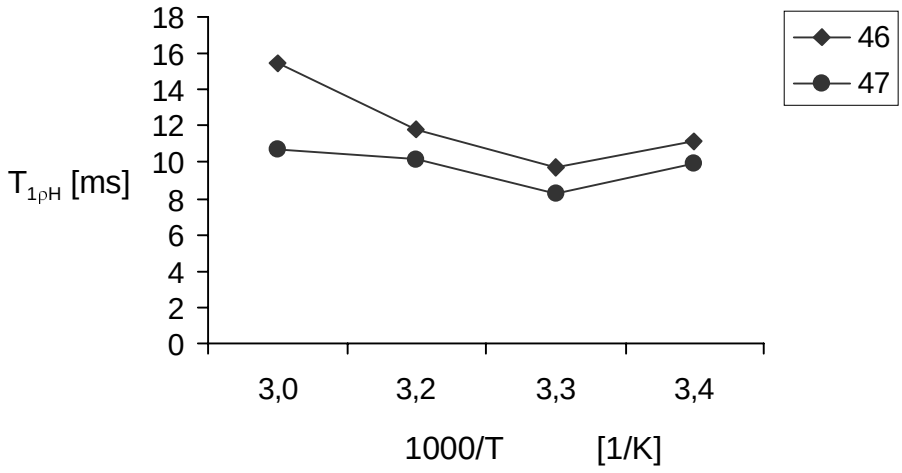

Figure 12. Temperature dependence of $T_{1\rho H}$ of **46** and **47** (see also Table 10).

Table 10. Temperature dependent $T_{1\rho H}$ data of **46** and **47**

Compound	$T_{1\rho H}$ [ms] [a]				relative cross–linkage	
	296 K	308 K	318 K	328 K	D	T
46	11.1	9.7	11.8	15.5	1.84	2.79
47	9.9	8.3	10.2	10.7	1.84	2.88

[a] Determined via ^{31}P CP/MAS NMR experiments.

3.1.4. Dynamic ^{2}H NMR Spectroscopy

Dynamic deuteron NMR measurements of compounds **80** – **83** have been carried out by the group of K. Müller, University of Stuttgart. Figure 13 shows four series of temperature-dependent ^{2}H NMR lineshapes for the inorganic–organic hybrid polymers **80**, **81**, **82**, and **83**. In the low temperature range, i.e. between 200 and 280 K, similar lineshape changes are observed that can be attributed to 180° ring flip motions of the deuterated phenylene rings. A closer inspection reveals distinct differences in the ^{2}H NMR lineshapes of the various samples depending on both the starting monomer and the solvent used during the polymer synthesis. The additional spectral narrowing, observed at temperatures above 280 K, indicate the onset of other motion(s) besides the ring flip process.

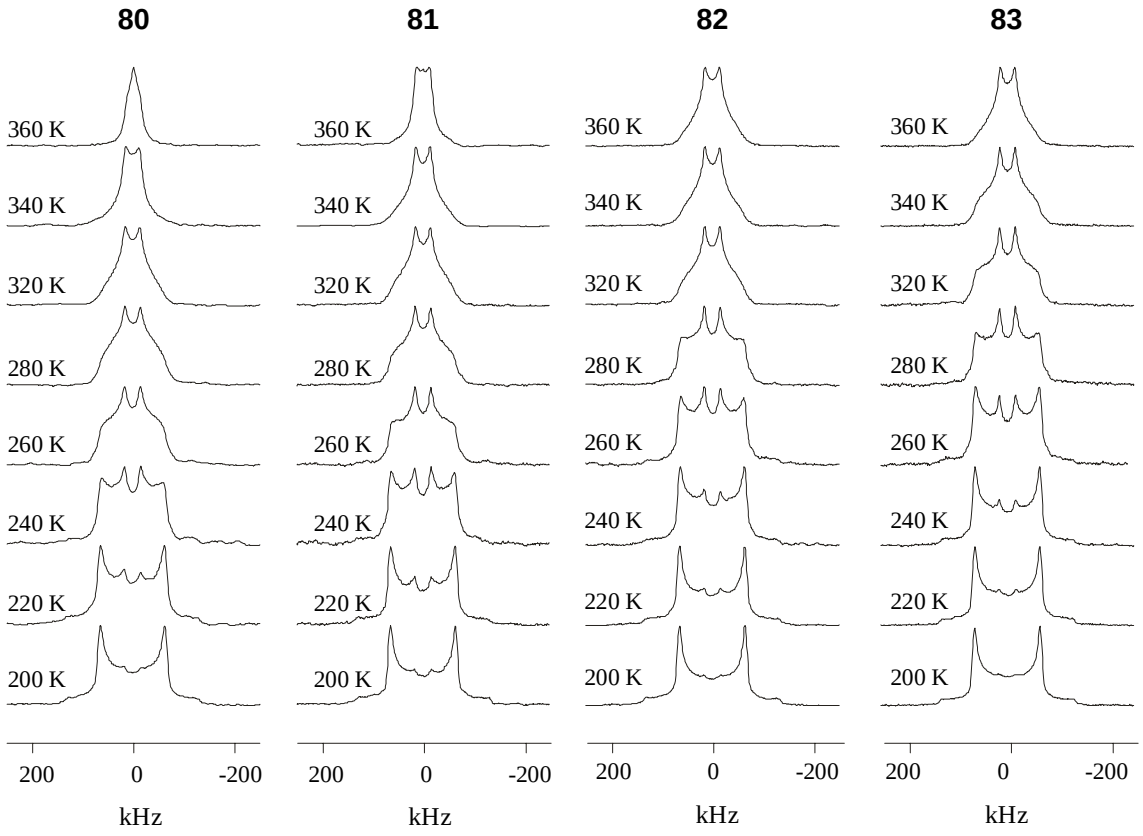

Figure 13. Experimental ^{2}H NMR lineshapes in dependence of temperature of **80** – **83**.

By comparing the ^{2}H NMR spectra of **80**/**81** and **82**/**83** the influence of the properties of the starting monomers can be estimated. It is found that in general the spectral changes of the T type polymers **82** and **83** occur at higher temperatures than those of the D type materials **80** and **81**. In addition, the overall spectral widths of the former samples are somewhat higher than those for the latter systems. Therefore, on a qualitative basis, **82** and **83** appear to be less mobile than **80** and **81**. This behavior is attributed to the different cross-linkage of these stationary phases (Tables 3 and 8).

In addition, it is found that the solvents THF and methanol, that were used during the sol–gel process, also have some effects on the observed ^{2}H NMR lineshapes. The influence of the solvent – although being relatively small – is mainly visible at temperatures above 300 K. For instance, at 340 K the overall spectral widths of the samples **80** and **82** (prepared in methanol) are smaller than the ones found in the corresponding spectra of **81** and **83** (prepared in THF). This again indicates a somewhat

higher mobility for the polymers synthesized in methanol than for those obtained from sol–gel processing in THF. The absolute order of mobility of the polymers **80** – **83** now can be stated; the mobility decreases in the sequence: **80** > **81** >> **82** > **83**.

From lineshape simulations up to 240 K the ^{2}H NMR signals of all polymers can be reproduced assuming a 180° flip motion of the phenylene rings. In the case of the most mobile polymeric matrix **80**, the dramatic narrowing of the lineshape at temperatures above 340 K leads to the assumption of additional motions – possibly an unhindered reorientation process of the whole chain system.[55,59]

3.1.5. ^{1}H HR/MAS and ^{13}C CP/MAS NMR Spectroscopy in the Suspended State

If inorganic–organic hybrid polymers are subjected to solvents that are able to induce swelling they enter an intermediate situation between the solid and the solution state which is designated as an interphase. As a consequence the mobility of molecular fragments and functional groups in the suspended state is increased exceeding by far the mobility of the material in the solid state. Therefore NMR spectra recorded in suspension of appropriate solvents (preferable deuterated NMR solvents) show a dramatic decrease in linewidths and an increase of resolution. The reason for this behavior is the 'simulation' of the solution state by fast motions of the polymer's functional groups carrying the nuclear spins, which results in largely reduced dipole–dipole interactions of the NMR active nuclei. The ^{1}H single pulse excitation (SPE)/MAS spectra of **73** suspended in CD_2Cl_2 and CD_3OD and the corresponding spectrum in the dry state are presented in Figure 14, in order to visualize this effect. Additionally, the influence of the polarity of the solvent on the swelling capability of the polymer matrix is visible. As a medium polar solvent dichloromethane (DCM) is able to induce a larger swelling of **73** than MeOH. This results in a higher mobility of the molecular fragments of **73** in the former solvent and in a better resolved ^{1}H NMR spectrum. The assignment of signals to the

corresponding functional groups is possible, especially in the case of **73** suspended in CD_2Cl_2 (Table 11).

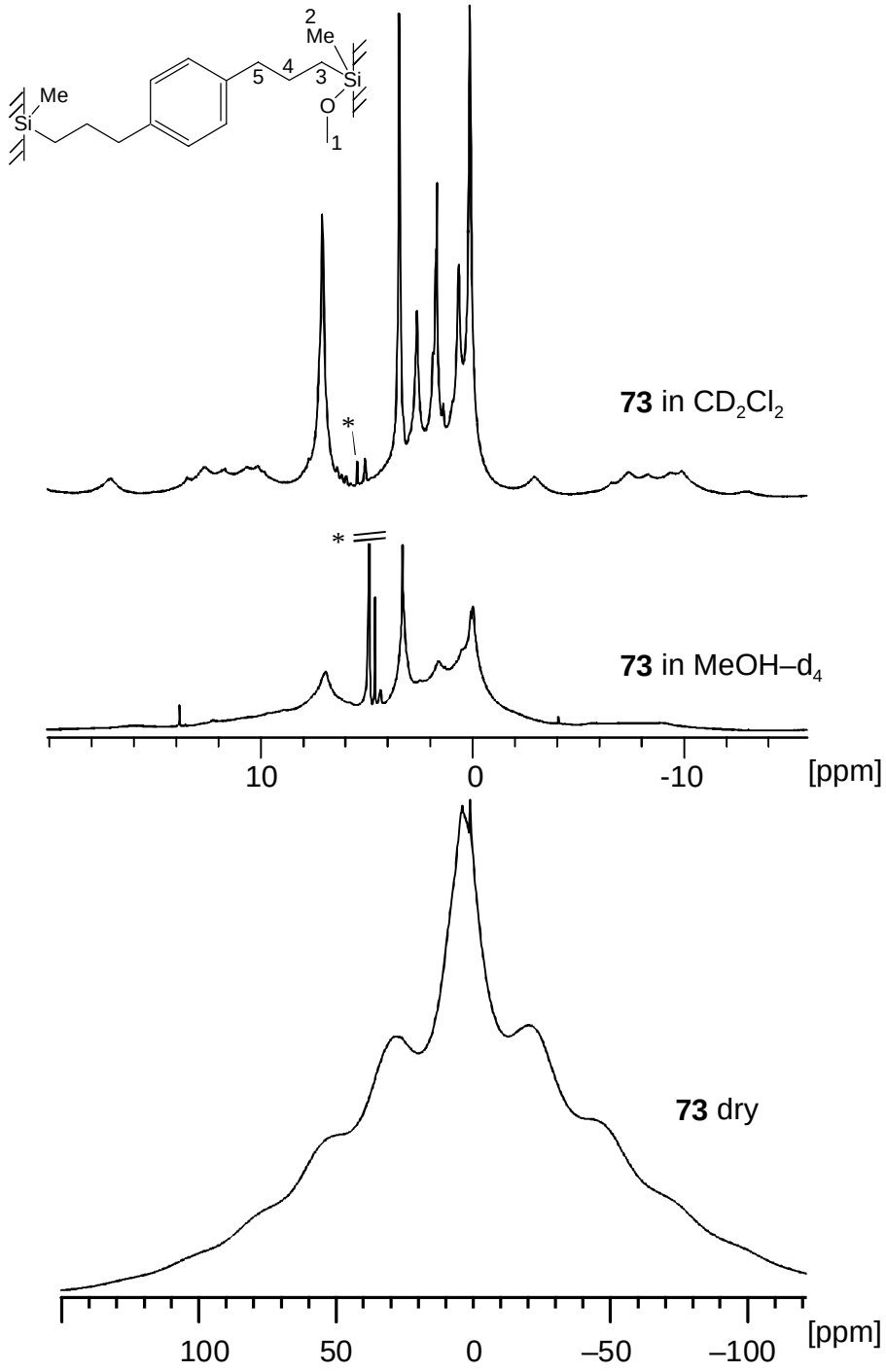

Figure 14. ^{1}H SPE/MAS spectra of **73** suspended in CD_2Cl_2 (top), MeOH–d_4 (middle), and in the dry state (bottom). *Solvent peaks; the solvent signal of CD_3OD is truncated (see also Table 11).

Table 11. ^{1}H chemical shift values of **73** suspended in CD_2Cl_2.

compound	δ ^{1}H [ppm] [a)]					
	H1	H2	H3	H4	H5	H arom.
73	3.3	0.1	0.5	1.6	2.4	6.9

[a)] For labeling see Figure 14 (top).

In Figure 15 the ^{1}H SPE/MAS spectrum of **46** – as an example of a phosphine functionalized copolymer – suspended in THF–d_8 is depicted. The most mobile functional groups of this material (methyl group of the D silyl species at 0 ppm, ethoxy group at 1.2 and 3.6 ppm) give rise to signals, that can be assigned to the corresponding sites easily.

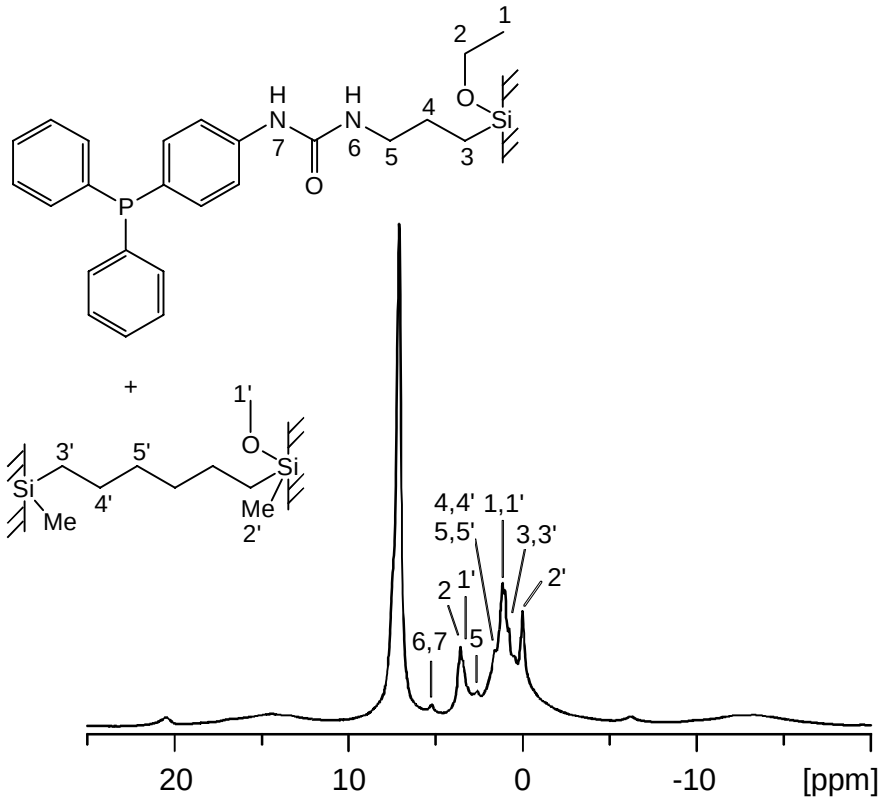

Figure 15. ^{1}H SPE/MAS spectrum of **46** suspended in THF–d_8.

As it was already mentioned (see chapter 2.1.2.2.), remaining dipole–dipole interactions between the protons of the suspended polymers can be utilized in order to perform ^{13}C CP/MAS NMR experiments on these interphases. In Figure 16 the ^{13}C CP/MAS NMR spectrum of **47** (suspended in CD_2Cl_2) is depicted.

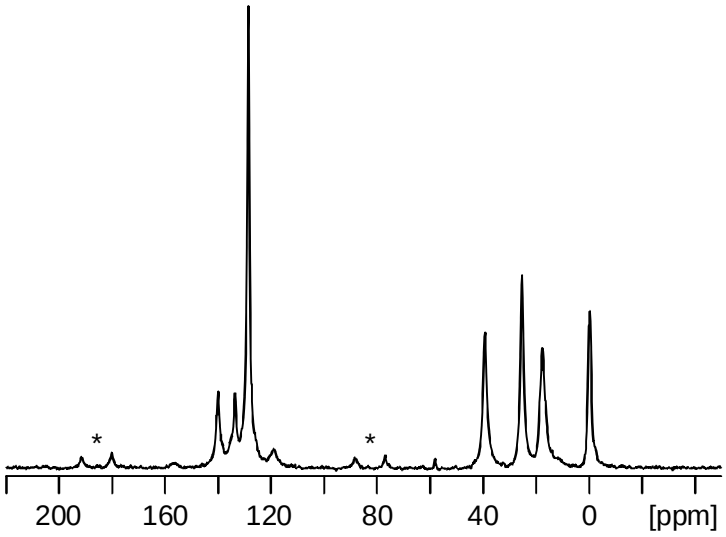

Figure 16. ^{13}C CP/MAS NMR spectrum of **47** suspended in CD_2Cl_2. *denotes rotational sidebands.

The improved resolution compared with the spectrum recorded in the dry state (Figure 5, bottom), especially in the aromatic region, is clearly visible.

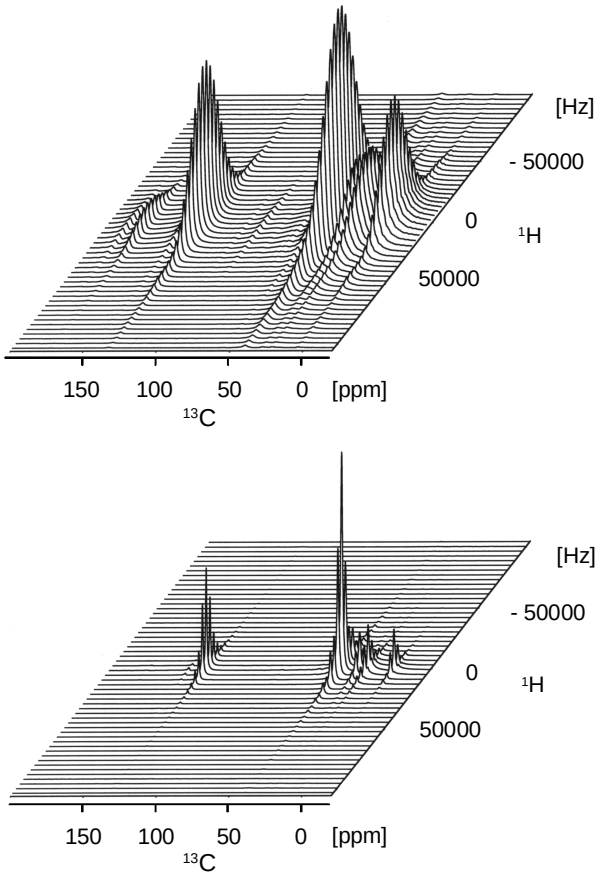

Figure 17. ^{13}C 2D WISE NMR spectra of **75** dry (top) and suspended in CD_2Cl_2 (bottom).

In order to visualize the gain of mobility if inorganic–organic hybrid polymers are suspended in solvents of suitable polarity the ^{13}C 2D WISE NMR spectra[60] of **75** in the dry state and suspended in DCM were recorded and are depicted in Figure 17. The decrease of the linewidth in the ^{1}H dimension averages to 50% which indicates a large increase of mobility of the polymeric matrix.

The ^{13}C CP/MAS NMR spectra of **80** – **83** suspended in DCM (Figure 18) visualize the differences of the swelling capabilities of D and T type polymers. The D type polymers **80** and **81** give rise to better resolved NMR spectra. This is the result of decreasing ^{1}H dipole–dipole interactions caused by larger swelling and a higher mobility compared to the behavior of the T type materials **82** and **83**.

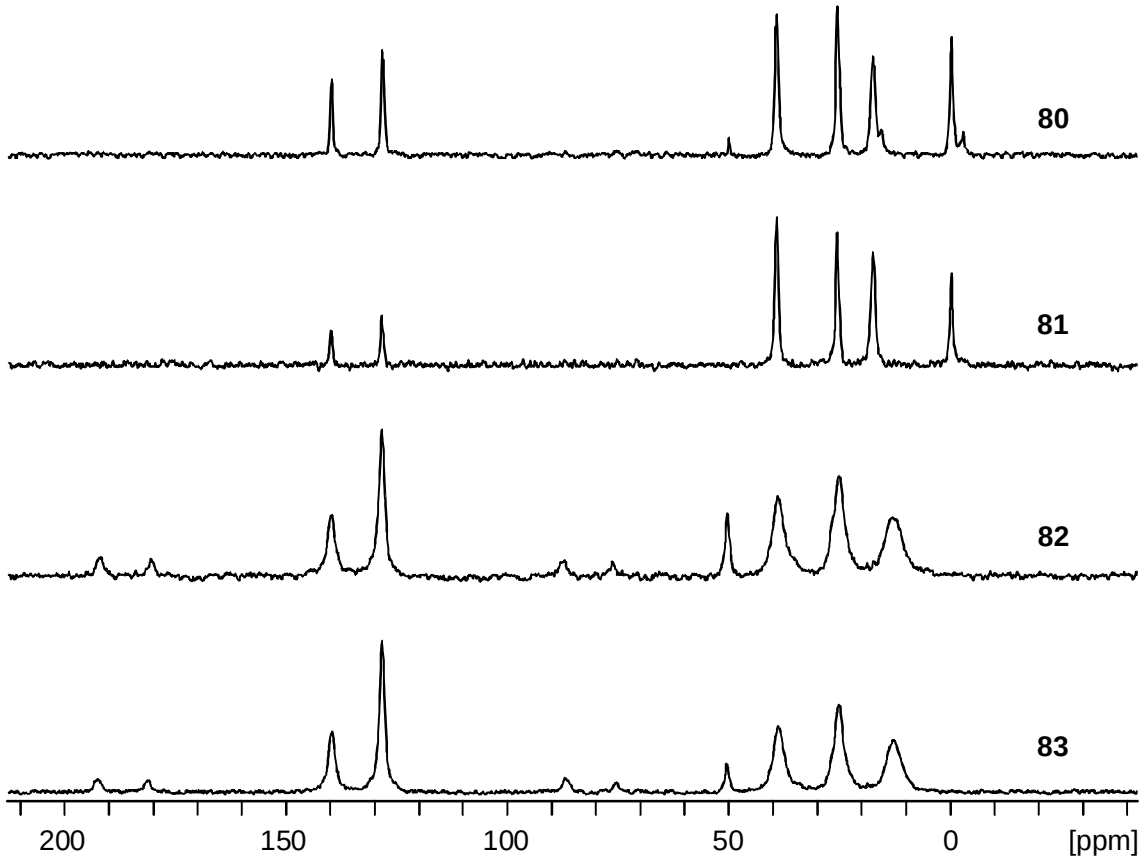

Figure 18. ^{13}C CP/MAS NMR spectra of **80** – **83** suspended in CD_2Cl_2.

3.1.6. Dynamic ^{1}H SPE/MAS NMR Spectroscopy

Since the inorganic–organic hybrid materials **73** – **84** should serve as co–condensing agents in the chemistry of interphases the knowledge about their dynamic behavior in the suspended state is of great importance. Therefore, $T_{1\rho H}$ measurements of these materials suspended in deuterated NMR solvents of different polarity (THF, DCM, and MeOH) have been performed. Additionally the phosphine functionalized copolymers **46** and **47** have been investigated by the same methods.

The relaxation times $T_{1\rho H}$ determined for different functional sites of the above mentioned suspended polymers are depicted in Figures 19 –24. Higher values of $T_{1\rho H}$ are indicating a higher mobility. The determined values of $T_{1\rho H}$ in dependence on the employed solvents and the investigated proton sites of the corresponding polymers are listed in detail in Tables 12 – 19. As previously mentioned MeOH – as a polar solvent – is not very well suited to induce swelling of the polysiloxane–based polymers **46**, **47**, **73**, **75**, and **80** – **83**. This results in very poor spectral resolution. Therefore, signals in the ^{1}H NMR spectra that could not be resolved were excluded from $T_{1\rho H}$ evaluations.

In general it is found that the mobilities of the methyl groups (only in D type polysiloxanes) and the non–hydrolyzed methoxy groups of the polymers increase most when being suspended, as it can be verified for example in Figures 19 and 20. Compounds **73** and **75** behave very similar, since they only differ in the length of the aliphatic chains (Table 1). The overall mobility of **73** is somewhat higher than that of **75**, which is the result of the somewhat lower degree of condensation of **73** (Table 3).

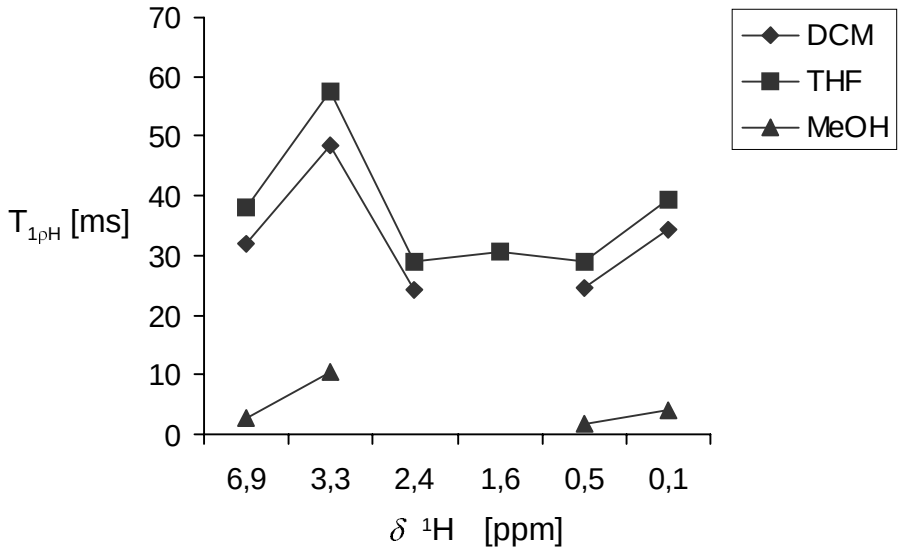

Figure 19. $T_{1\rho H}$ values of **73** in dependence of the ^{1}H chemical shifts determined in suspensions of different solvents (see also Table 12).

Table 12. $T_{1\rho H}$ data of **73** determined in suspension of different solvents

solvent	$T_{1\rho H}$ [ms]					
	6.9 ppm	3.3 ppm	2.4 ppm	1.6 ppm	0.5 ppm	0.1 ppm
DCM	32.0	48.4	24.3	[a]	24.5	34.2
THF	38.1	57.7	28.8	30.8	28.8	39.5
MeOH	2.8	10.5	[a]	[a]	1.8	4.8

[a] Not determined because of poor swelling and resulting low spectral resolution.

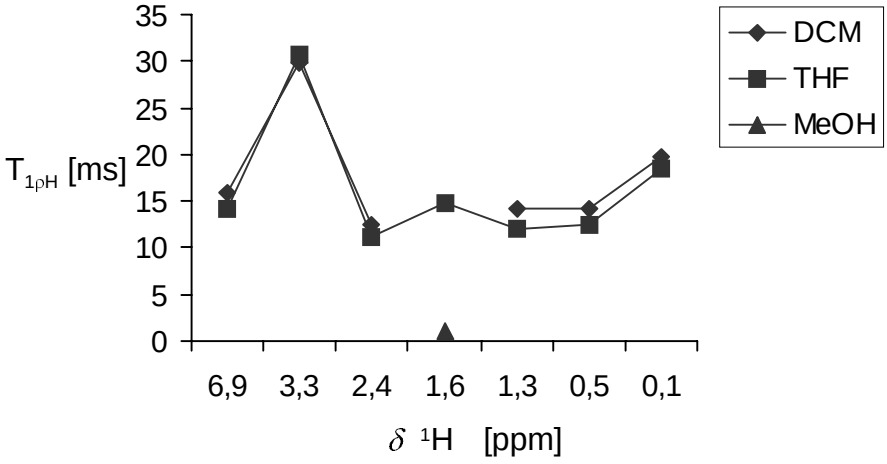

Figure 20. $T_{1\rho H}$ values of **75** in dependence of the ^{1}H chemical shifts determined in suspensions of different solvents (see also Table 13).

Table 13. $T_{1\rho H}$ data of **75** determined in suspension of different solvents

solvent	$T_{1\rho H}$ [ms]						
	6.9 ppm	3.3 ppm	2.4 ppm	1.6 ppm	1.3 ppm	0.5 ppm	0.1 ppm
DCM	15.9	29.8	12.5	[a]	14.2	14.2	19.7
THF	14.2	30.7	11.1	14.7	12.1	12.5	18.5
MeOH	[a]	[a]	[a]	1.2	[a]	[a]	[a]

[a] Not determined because of poor swelling and resulting low spectral resolution.

The stationary phases **80** and **81** (Figure 21 and Tables 14 and 15) show a slightly different behavior than their non–deuterated derivative **73**. The methylene group in the middle of the aliphatic chain (at 1.6 ppm) is clearly more mobile than the neighbors, as expected.

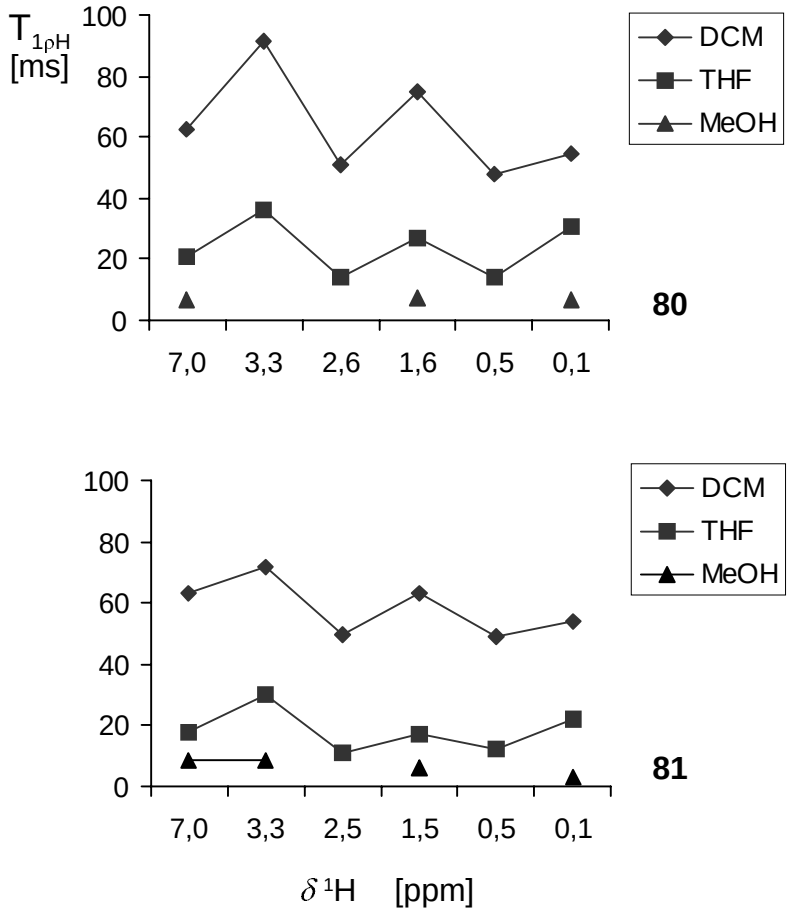

Figure 21. $T_{1\rho H}$ values of **80** (top) and **81** (bottom) in dependence of the ^1H chemical shifts determined in suspensions of different solvents (see also Tables 14 and 15).

Until now there is no simple explanation why this is not the case for the polymers **73** and **75**. Possibly the lower degrees of condensation of **73** (and also **75**) lead to different motional modes, i.e. exciting other resonance frequencies of the monomeric building blocks of **73** and **75**.

Table 14. $T_{1\rho H}$ data of **80** determined in suspension of different solvents

solvent	$T_{1\rho H}$ [ms]					
	7.0 ppm	3.3 ppm	2.6 ppm	1.6 ppm	0.5 ppm	0.1 ppm
DCM	62.3	91.3	50.7	74.7	48.0	54.5
THF	21.0	36.4	14.0	27.0	14.0	30.5
MeOH	6.5	[a]	[a]	7.1	[a]	6.5

[a] Not determined because of poor swelling and resulting low spectral resolution.

Table 15. $T_{1\rho H}$ data of **81** determined in suspension of different solvents

solvent	$T_{1\rho H}$ [ms]					
	7.0 ppm	3.3 ppm	2.5 ppm	1.5 ppm	0.5 ppm	0.1 ppm
DCM	63.0	72.0	50.0	63.0	49.0	54.0
THF	18.0	30.0	11.0	17.0	12.0	22.0
MeOH	8.3	8.5	[a]	6.0	[a]	3.0

[a] Not determined because of poor swelling and resulting low spectral resolution.

As examples for only T type polymers **82** and **83** show the expected reduced swelling capacity compared to **80** and **81**. The corresponding values for $T_{1\rho H}$ are much lower than those determined for the D type polymers with the same chain length, as it can be verified in Figure 22 as well as in Tables 16 and 17 (for purposes of visualization the scale of the ordinates in Figure 22 have not been changed). Additionally it is found that swelling and mobility of the T type materials are larger in suspensions of THF than in those of DCM. The $T_{1\rho H}$ values determined in DCM and MeOH interphases of **82** and **83** resemble those found by measurements in the solid state (see values at 296 K in Table 8), which indicates a rather rigid behavior in these solvents.

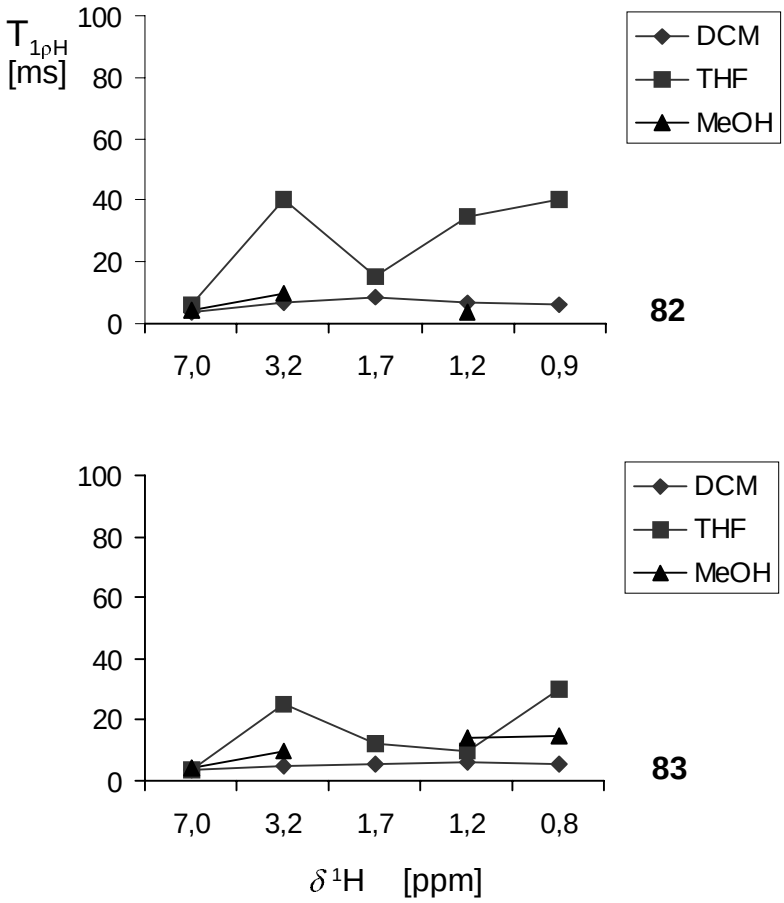

Figure 22. $T_{1\rho H}$ values of **82** (top) and **83** (bottom) in dependence of the ^{1}H chemical shifts determined in suspensions of different solvents (see also Tables 16 and 17).

Table 16. $T_{1\rho H}$ data of **82** determined in suspension of different solvents

solvent	$T_{1\rho H}$ [ms]				
	7.0 ppm	3.2 ppm	1.7 ppm	1.2 ppm	0.9 ppm
DCM	3.9	6.5	8.8	7.0	6.0
THF	6.2	40.0	15.0	35.0	40.0
MeOH	4.4	9.5	[a]	3.9	[a]

[a] Not determined because of poor swelling and resulting low spectral resolution.

Table 17. $T_{1\rho H}$ data of **83** determined in suspension of different solvents

solvent	$T_{1\rho H}$ [ms]				
	7.0 ppm	3.2 ppm	1.5 ppm	1.2 ppm	0.8 ppm
DCM	3.6	4.9	5.7	6.3	5.6
THF	3.8	25.0	12.0	10.0	30.0
MeOH	4.2	10.0	[a]	14.0	15.0

[a] Not determined because of poor swelling and resulting low spectral resolution.

Polymer **84** shows a good swelling behavior in the medium polar solvents THF and DCM and the expected bad swelling in MeOH (Figure 23 and Table 18). The mobility of the phenyl ring bound to the silicon atom (7.0 ppm) does not exceed the mobility of the aliphatic chain. Obviously the steric hindrance is too big to allow faster motions, compared to the methyl groups of the other D type polymers.

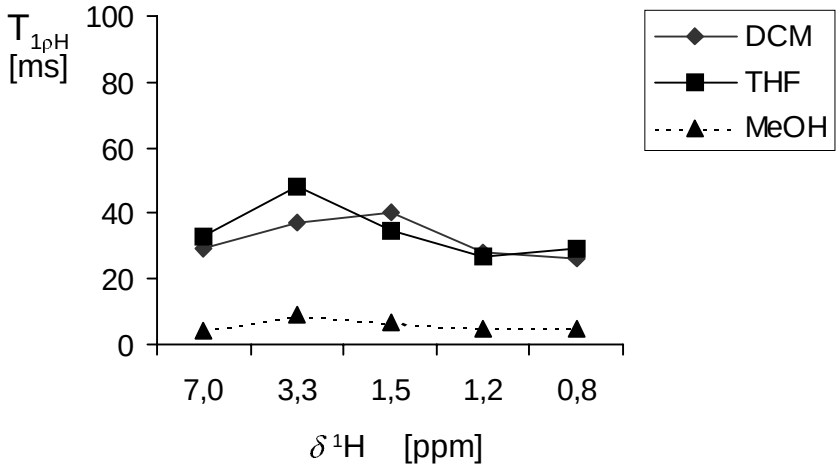

Figure 23. $T_{1\rho H}$ values of **84** in dependence of the ^{1}H chemical shifts determined in suspensions of different solvents (see also Table 18).

Table 18. $T_{1\rho H}$ data of **84** determined in suspension of different solvents

solvent	$T_{1\rho H}$ [ms]				
	7.0 ppm	3.3 ppm	1.5 ppm	1.2 ppm	0.8 ppm
DCM	29.0	37.0	40.0	28.0	26.0
THF	33.0	48.0	35.0	27.0	29.0
MeOH	4.0	9.0	7.0	5.0	5.0

[a)] Not determined because of poor swelling and resulting low spectral resolution.

The findings for the phosphine functionalized polymers **46** and **47** are very interesting (Figure 24 as well as Tables 19 and 20). The most mobile functional groups are the non–hydrolyzed ethoxy group and the protons of the aromatic systems, as well as the methyl group of the D type co–condensing agent. Most rigid are the amide protons of the urea group and those of the neighbored methylene function. The high mobility of the triphenylphosphine fragment is surprising; despite the rigid urea group and the short

propyl chain it reaches the mobility of the small and flexible non hydrolyzed ethoxy groups (Figure 24). Since this is the case concerning all three employed solvents this effect seems to be based on the fact that the polymers are suspended, rather than on the polarity of the solvents. The $T_{1\rho H}$ values of the MeOH interphases of **46** and **47** can be determined without complications. These materials reveal sufficient swelling and good resolved spectra, although the degrees of condensation of the D and the T groups of both of the polymers are very high. Possibly the polarity of the urea group plays a major part in the interaction of swelling and mobility of **46** and **47** in MeOH by increasing the acceptance for this polar solvent.

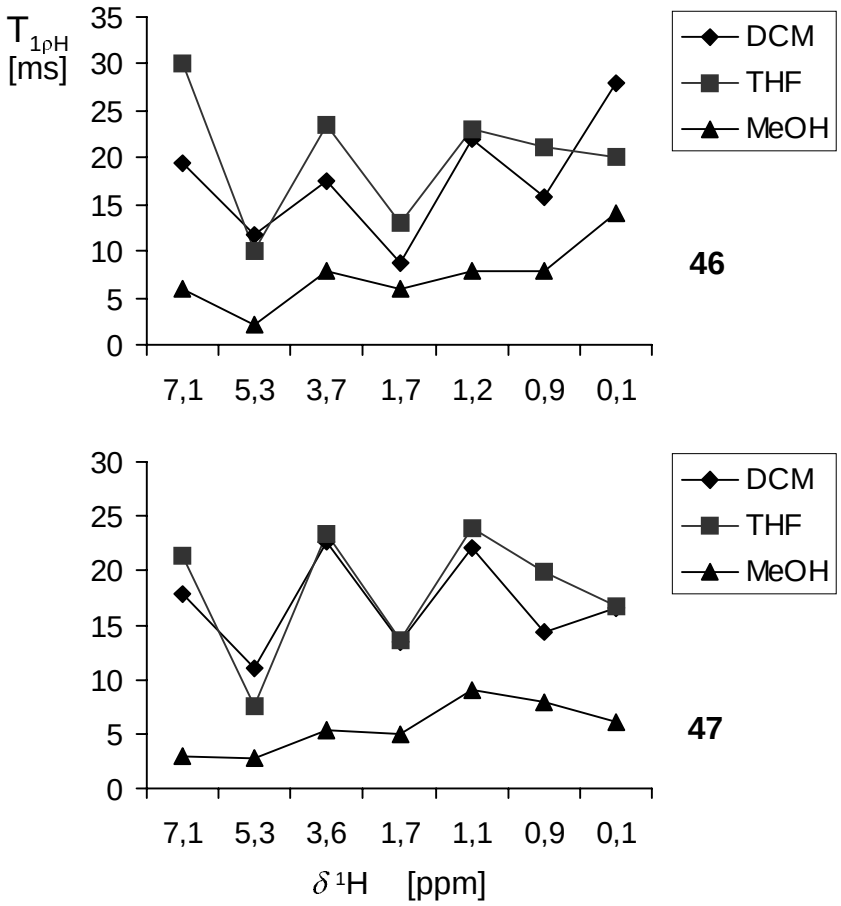

Figure 24. $T_{1\rho H}$ values of **46** (top) and **47** (bottom) in dependence of the ^{1}H chemical shifts determined in suspensions of different solvents (see also Tables 19 and 20).

On a qualitative basis, concerning the average $T_{1\rho H}$ values determined in suspensions, **46** (**D^0–$(CH_2)_6$–D^0** as co–condensing agent) is assumed to be slightly more mobile than **47** (**D^0–$(CH_2)_3$–(C_6H_4)–$(CH_2)_3$–D^0** as co–condensing agent) which agrees with the findings of the temperature dependent measurements (see chapter 3.1.3.).

Table 19. $T_{1\rho H}$ data of **46** determined in suspension of different solvents

Solvent	$T_{1\rho H}$ [ms]						
	7.1 ppm	5.3 ppm	3.7 ppm	1.7 ppm	1.2 ppm	0.9 ppm	0.1 ppm
DCM	19.5	11.8	17.5	8.8	22.0	15.7	28.0
THF	30.0	10.0	23.5	13.0	23.0	21.2	20.0
MeOH	6.0	2.1	8.0	6.0	8.0	8.0	14.0

Table 20. $T_{1\rho H}$ data of **47** determined in suspension of different solvents

solvent	$T_{1\rho H}$ [ms]						
	7.1 ppm	5.3 ppm	3.6 ppm	1.7 ppm	1.1 ppm	0.9 ppm	0.1 ppm
DCM	17.8	11.1	22.6	13.5	22.1	14.4	16.6
THF	21.4	7.6	23.3	13.6	24.0	18.8	16.7
MeOH	3.0	2.8	5.4	5.0	9.0	8.0	6.0

3.2. Evaluation of NMR Spectroscopic Derived Dynamic Parameters by Kohonen's Self Organizing Feature Map

The application of the Kohonen map (SOM) proved to be a suitable method for the visualization of the NMR relaxation time data (Table 2, entries **1** – **72**). A large number of inorganic–organic hybrid polymers (Table 1, entries **1** – **72**), that cannot be compared to each other directly, were evaluated and sorted. Instead of numerous two–dimensional diagrams, one map including all information was obtained (Figure 25).

The nonlinear topology–preserving Kohonen map showed clear advantages over traditional statistical methods like principle component analysis (Figure 26). Regarding the scatter plot of the first two principle components, the identification of two or three clusters may be possible but it is not suitable for further interpretation.

Since a very large Kohonen map was chosen for visualization, the Euclidean distances between neighboring neurons are rather small; therefore, these distances or the derived u–matrix cannot be used to identify clusters automatically. Regarding the u–matrix–map (Figure 27), no large white regions and no sharp borders are found. This indicates that a huge variety of compounds is distributed over big parts of the data space. Expert know–how is required to interpret and validate the map. As soon as it is reduced to sizes that are usually used for classification, similar substances will be located on the same neuron and a good separation with larger Euclidean distances is obtained – in this case clusters can be identified easily (Figure 28). Comparing the smaller Kohonen map with the one that was applied for visualization, it is possible to verify whether any disadvantages or even errors have been acquired by employing such a large map. As it can be verified in Figures 28 and 25, the small map agrees with the larger one, since there is almost the same ordering (apart from being rotated or mirrored which does not have any effect on the neighborhood relationships or the distribution).

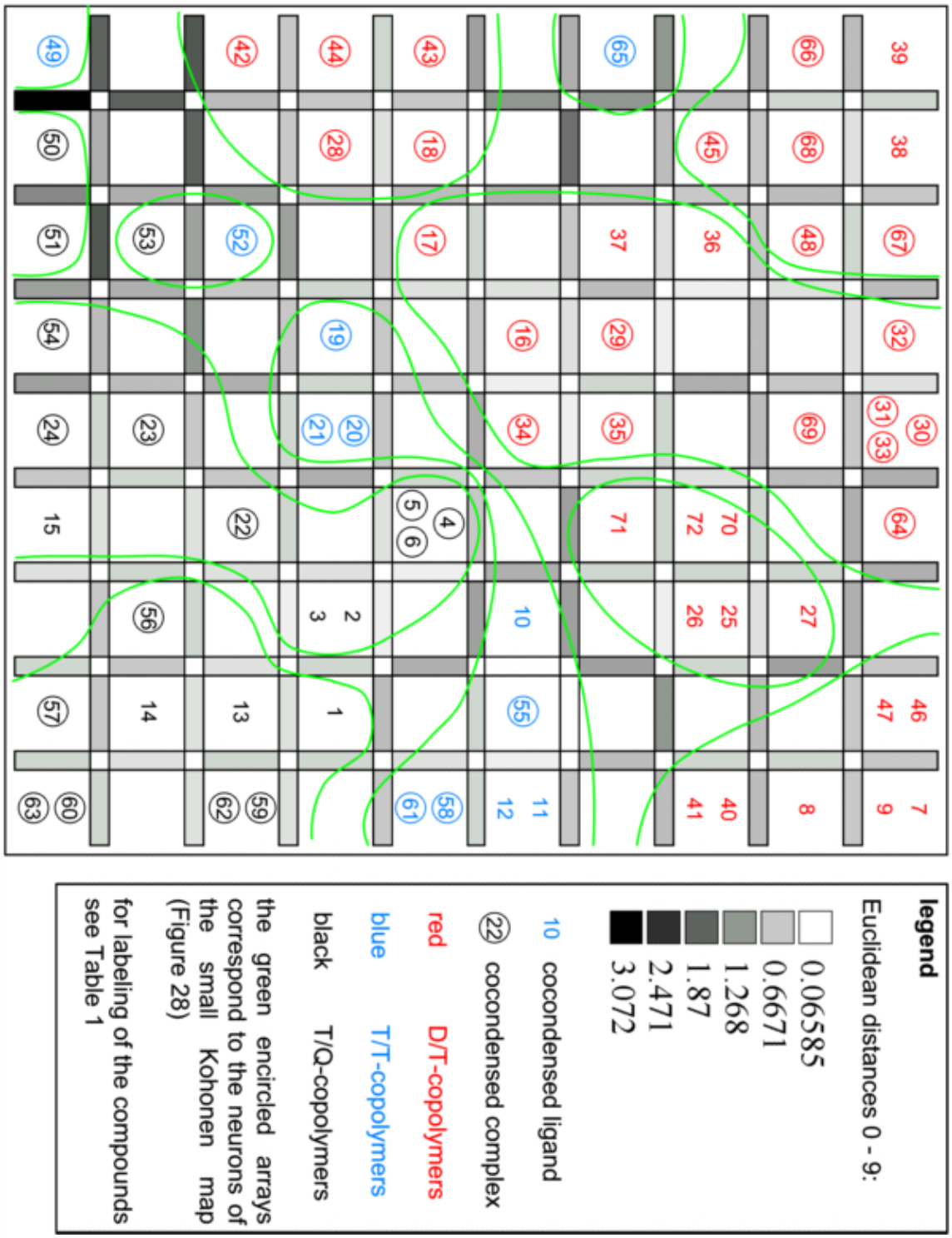

Figure 25. Combined large (10 × 9 neurons) Kohonen and distance map visualizing the evaluation of the NMR relaxation time data of **1** – **72**.

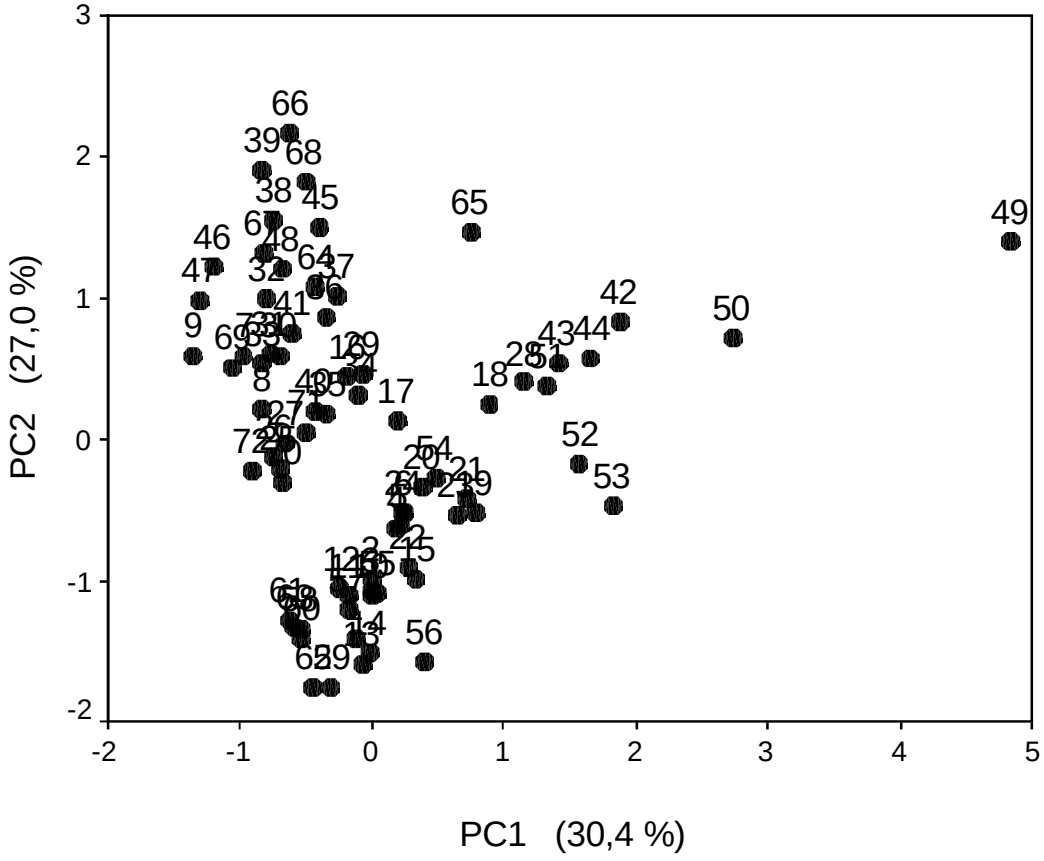

Figure 26. Results of the principle component analysis of **1** – **72**.

Despite the fact that the maps were initialized randomly and the data were sorted randomly at the beginning of the training, a great reproducibility is found. The only notable differences that were observed between several independent runs with the same data, were mirrored or rotated maps, which do not affect the results.

The main criterion the compounds are sorted by the ANN is the presence or absence of values for the degree of condensation of the D–, T–, or Q–groups. Accordingly the output of the SOM is divided into three main sections, the D–, T–, and Q–domains (Figure 25). It is remarkable that the D– and Q–domains are separated by a strip of only T–co–condensed compounds. In fact, the 'T–only' co–condensed polymers show physical and chemical properties which range between those of the D and the Q functionalized polymers, e.g. the degree of connectivity, or the dynamic behavior.

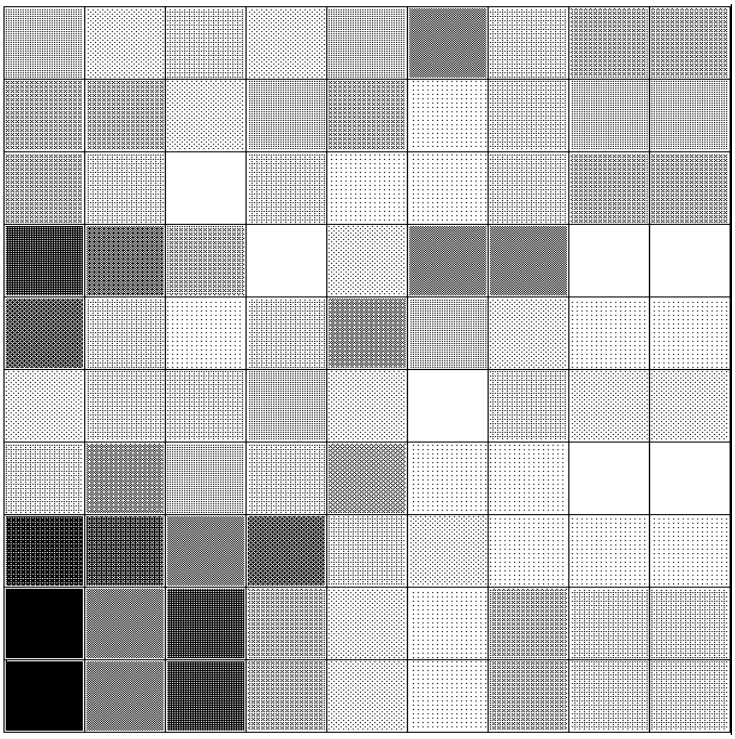

Figure 27. Unified matrix (u–matrix) visualizing the clustering of **1 – 72** on the large SOM. The top left neuron corresponds to the 'entry **39 neuron**' in Figure 25.

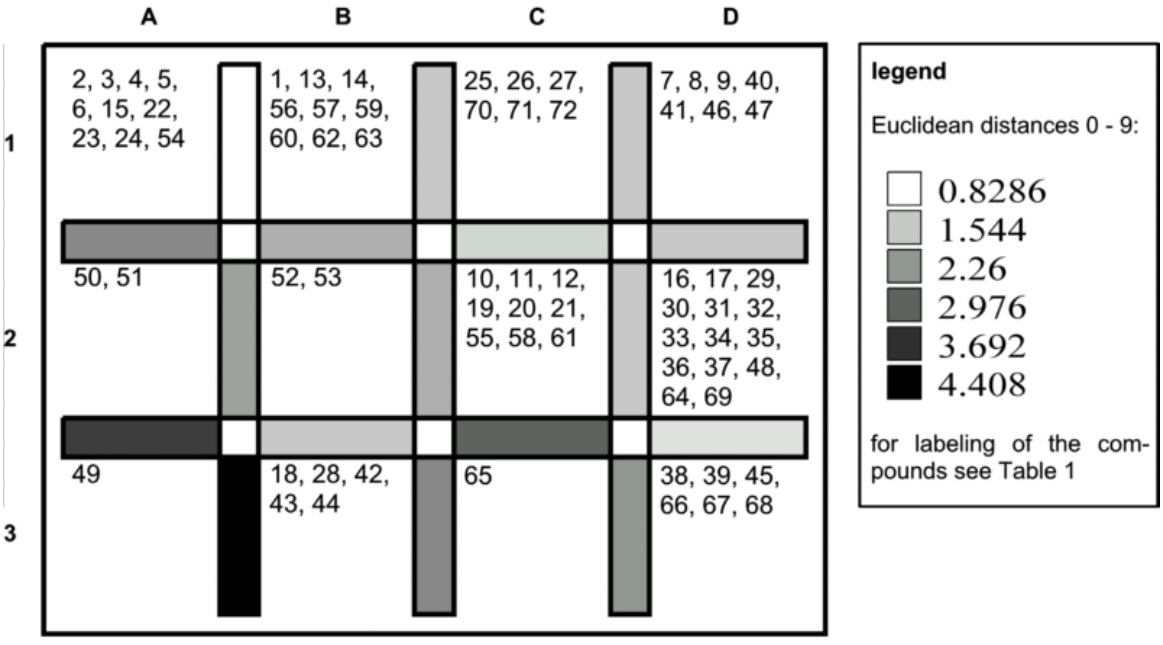

Figure 28. Combined small (4 × 3 neurons) Kohonen and distance map. Compared to Figure 25 this map is mirrored along the diagonal from bottom left to top right.

The composition of the three different domains is determined by all ten NMR parameters and it is not straightforward to decide which are the most significant. The distribution maps of the $T_{1\rho H}$ values measured by ^{29}Si or ^{31}P CP/MAS NMR spectroscopy respectively, appear very similar (Figure 29). High $T_{1\rho H}$ values reside in the upper left part of the Kohonen map, while the lowest $T_{1\rho H}$ values are positioned in the lower right part.

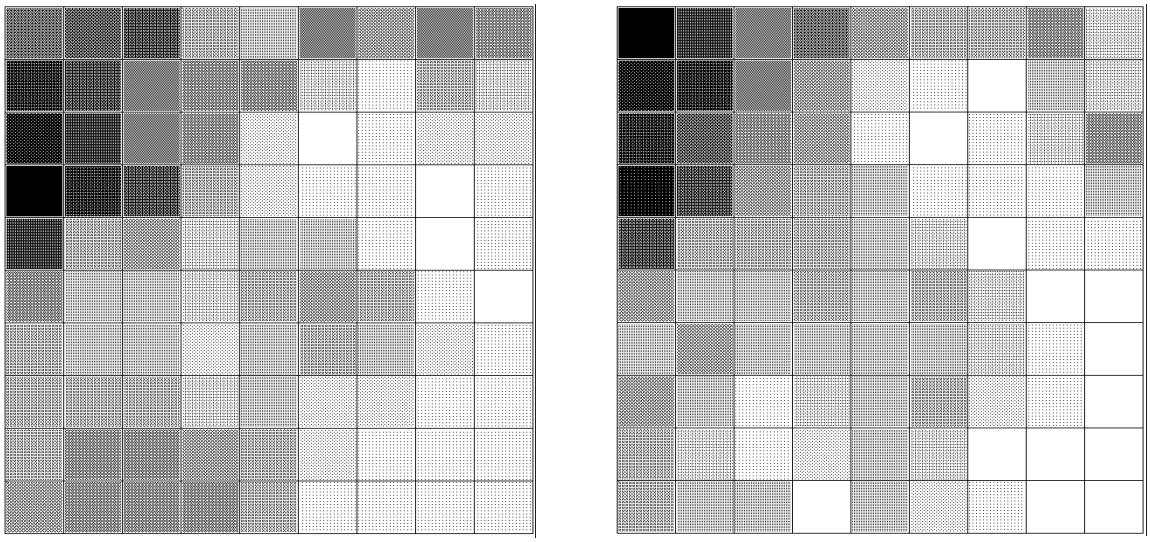

Figure 29. Distribution–maps of $T_{1\rho H}$(P) (left) and $T_{1\rho H}$(Si) (right) corresponding to the large SOM (Figure 25). The top left neurons correspond to the 'entry **39** neuron' in Figure 25.

By way of contrast, the highest T_{PH} values are found in the upper right of the map (see Figure 25 and 30). Thus the main criteria for the arrangement within the D–domain are the relaxation times T_{PH} and $T_{1\rho H}$. A related sorting phenomenon is found in the T– and the Q–domains. The degree of condensation of the T–groups is a parameter that equally applies to all evaluated polymers. It influences mainly the position of the Q–type polymers on the map, but in a more subordinate way than the values of the relaxation times do. Very low degrees of condensation of the T–groups are found in the lower left, while the highest degrees of condensation are found on the right side of the Kohonen map, with the main focus on the lower right side (Figure 31).

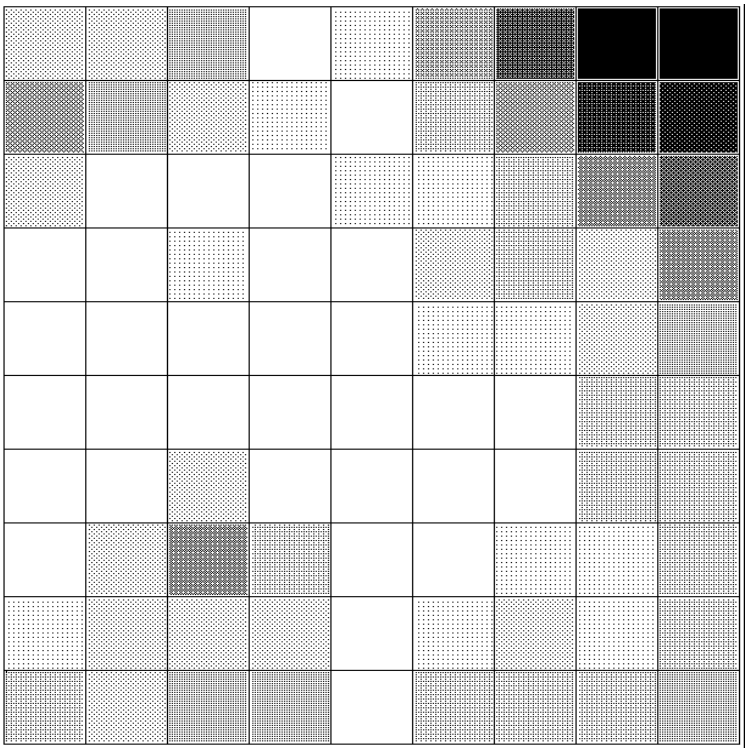

Figure 30. Distribution map of the T_{PH} values of **1 – 72** (see Table 2) corresponding to the large SOM (Figure 25). The top left neuron corresponds to the 'entry **39** neuron' in Figure 25.

39	38	67	32	30,31 33	64		46	47	7	9
66	68	48		69		27			8	
	45	36			70,72	25, 26			40,41	
65		37	29	35	71					
			16	34		10	55		11,12	
43	18	17			4,5 6				58,61	
44	28		19	20,21		2, 3	1			
42		52			22		13		59,62	
		53		23		56	14			
49	50	51	54	24	15		57		60,63	

Figure 31. Distribution–map of the degrees of condensation of the T–groups. Light gray: degrees of condensation < 75 %; dark gray: degrees of condensation > 95 %.

Most of the co–condensed ligands appear on the upper right half of the large Kohonen map (Figure 25) while the polymers containing co–condensed complexes mainly occupy the lower and the left half. To explain this fact the dynamic behavior of all compounds has to be taken into account. When the mobility of the polymers increases, the process of magnetization transfer becomes slower and the T_{PH} values increase (see chapter 2.1.2.1.). In general co–condensed ligands are more mobile than co–condensed complexes, therefore ligands should be located in regions of the map in which the highest T_{PH} values are found (Figures 25 and 30). In particular this is the case for the D–domain on the Kohonen map, but also in the T– and the Q–domains a concentration of ligands in specific areas is present.

The distribution of the polymers on the Kohonen map is influenced by their structural and dynamic properties which are partially a result of the sol–gel process applied. The way the sol–gel process proceeds depends on many different factors, like solvent employed, hydrolytic or non–hydrolytic route, concentration of the reaction partners, applied temperature, and others.[6,8,61] The low range order within the polymers in the vicinity of the metal centers and the functional groups of the ligands is determined additionally by the molecular shape and the polarity of the educts. This may lead to template effects, especially in the surroundings of functional groups, which will be approximately the same if similar starting materials are employed for the sol–gel process. Therefore the steric, structural, and dynamic (NMR) parameters of polymers prepared in such a way must be roughly the same. The Kohonen map expresses this fact – without having information about structural features of the polymers – by placing materials with similar structures in close vicinity on the map or even on the same neuron, as for example this is the case for compounds **1** and **13**, **4** – **6**, **7** and **9**, or **59** and **62** (see more examples in Table 1 and Figure 25). The type of co–condensing agent and especially its stoichiometric amount in the polymer plays a major role regarding the physical properties

of the polymers. This is the reason why **18** and the compounds **16** and **17** are separated on the small map although their chemical structures are almost identical. The same is true for compounds **49** and **50**/**51**. In addition, **49** shows the lowest degree of condensation of the 'T–only' co–condensed polymers which leads to a significant different pattern of signal intensities T^0 – T^3 in the ^{29}Si NMR spectra, compared to the adjacent polymers **50** and **51**. This fact explains the high Euclidean distances between these neighboring substances and the 'isolation' of **49**. In contrast, the above explanation does not apply to compounds **1**, **2**, and **3**. In these cases the structure of the co–condensed ligand is the decisive factor separating them on the small map. The larger functional groups connected to the phosphine centers like tetrahydrofuranyl and dioxanyl in **2** and **3** versus methoxyethyl in **1** lead to a smaller mobility of the former two polymers and higher $T_{1\rho H}$ values for **2** and **3** compared to **1**. The exposed position of compound **65** on the map is explained by the remarkable high values of $T_{1\rho H}$ and the low value of T_{PH}. Although this system is a 'T–only' co–condensed polymer and the phosphine centers are anchored to the matrix by only one spacer it is one of the most rigid polymers presented in this work. The high Euclidean distances to the neighbors and its somewhat isolated position on the map reflect this fact.

The accumulation of similar structural characteristics of the compounds residing on neuron C2 of the small map (Figure 28) is noteworthy. In this T–domain cluster trisphosphine complexes are gathered (**19** – **21** and **55**, **58**, **61**), likewise the ligands **10** – **12** forming the complexes **19** – **21** are present. The combination of these characteristics (trisphosphine complexes and the same or similar ligands) leads to polymers with similar dynamic properties. An analogous case is found on neuron D1, but the overlap of characteristics is not as obvious as in the former case. The main feature of these polymers (**7** – **9**, **40**, **41**, **46**, and **47**) assembled in this cluster is the representation of monodentate phosphine ligands. These compounds show similar molecular dynamics, although they

were prepared with three different co–condensing agents (Table 1) and although the phosphine centers in **40** and **41** are double spaced, which is in contrast to the single spaced phosphines **7** – **9**, **46,** and **47**. Another interesting fact regarding these latter polymers is their relation between mobility and structure. Compounds **7** – **9** each were provided with different spacer lengths from n = 3 to n = 8, but were co–condensed with the simple co–condensing agent $(H_3C)Si(OCH_3)_3$ (**D^0**). In contrast the spacers in **46** and **47** are build up by a propyl chain and a rigid urea group and both phosphine ligands are co–condensed with D type monomers of nearly the same flexibility (see Table 1). Nevertheless the mobility of **7** – **9**, **46,** and **47** in the dry state is nearly the same. This leads to the conclusion that even rigid molecules can be 'mobilized' by co–condensing them with an appropriate co–condensing agent.

It is remarkable to see that many polymers, which are found in close vicinity on both of the Kohonen maps and which share similar but not equal structural features, create similar sets of dynamic NMR data (e.g. **58** and **61**, **59** and **62**, or **60** and **63**). These results give evidence that specific physical properties, like a high or a low mobility, is achieved by different ways of modification of the polymers. For example the introduction of long hydrocarbon spacers in the ligands or in the co–condensing agents and or the choice of D–type co–condensing agents leads to highly mobile polymers.[18,22] On the other hand, if rigid systems are favored the way of spacing (two– or threefold) or the application of other types of co–condensing agents (T–type or Q–type) are possible methods of polymer modification (examples for rigid systems are the polymers **4** – **6**, **22** – **24**, or **42** – **45**, examples for highly mobile systems are the polymers **7** – **9**, **25** – **27**, **40**, **41**, **46**, **47**).

4. Conclusions

4.1. Mobility Studies on Inorganic–Organic Hybrid Polymers

The results of the solid state NMR measurements of the mixed type copolymers **46** – **48** and **76** – **79** demonstrate that in each case the initial stoichiometries have been retained during the sol–gel processing. Compound **73** proves to be an appropriate co–condensing agent for transition metal complexes or phosphine ligands in order to build stationary phases for chemistry in interphases, as it was proved by synthesizing **46** – **48**. In each case (**46** – **48**, **73** – **84**) the determination of only one value for $T_{1\rho H}$ in the solid state leads to the conclusion that the relaxation mechanisms are spin–diffusion controlled and that no domains are formed while sol–gel processing. The temperature dependent measurements of $T_{1\rho H}$ allow only qualitative comparisons concerning the mobilities of **46** – **48** and **73** – **84**. ^{2}H NMR experiments confirm the close relationship between the mobility of a polymeric matrix, its starting materials (D or T type) and the solvent used for the sol–gel process. They allow also the qualitative rating of the mobilities of the deuterated polymers **80** – **83**. Determinations of $T_{1\rho H}$ in interphases of **46**, **47**, **73**, **75**, and **80** – **83** reveal that the mobility of these polymers is increased by order of magnitudes depending on the polarity of the solvent employed.

4.2. Evaluation of NMR Spectroscopic Derived Dynamic Parameters

Different inorganic–organic hybrid polymers (Table 1, entries **1** – **72**) with a variety of structural features are evaluated by the Self–Organizing Feature Map first implemented by Kohonen. Ten solid state NMR derived dynamic parameters (Table 2) of each compound are used as an input for the Artificial Neural Network. The results of approximately 100000 training steps are visualized by Kohonen maps of different size and supported by distribution maps concerning the most important dynamic parameters ($T_{1\rho H}$, T_{PH}, etc).

5. Experimental Section

5.1. Solid State NMR Measurements

The solid state NMR spectra were recorded on Bruker DSX 200 and Bruker ASX 300 multinuclear spectrometers equipped with wide bore magnets (field strengths of 4.7 T and 7.05 T). Magic angle spinning was applied up to 10 kHz (4 mm ZrO_2 rotors) and 3 – 5 kHz (7 mm ZrO_2 rotors). Frequencies and standards: ^{13}C, 50.288 MHz (4.7 T), 75.432 MHz (7.05 T), [TMS, carbonyl resonance of glycine (δ = 176.0) as secondary standard]; ^{29}Si, 39.73 MHz (4.7 T), 59.595 MHz (7.05 T), (Q_8M_8, as secondary reference); ^{31}P, 80.961 MHz (4.7 T), 121.442 MHz (7.05 T) [85% H_3PO_4, $NH_4H_2PO_4$ (δ = 0.8) as a secondary reference]. The cross polarization constants T_{CH}, T_{SiH}, and T_{PH} were determined by variations of the contact time T_c (14 – 16 experiments). The proton relaxation times in the rotating frame were measured by direct proton spin lock–τ–CP experiments according to ref.[37] The relaxation parameters were obtained using the Bruker software SIMFIT and WIN–FIT following the procedure explained in this thesis (chapter 2.1.2.1.) and given in ref.[18,20] In this references also the parameters for the 2D WISE NMR experiments were described.

5.2. Suspension State NMR Measurements

The HR/MAS suspension state NMR spectra were recorded on a Bruker ARX 400 spectrometer equipped width a standard bore magnet (field strength 9.4 T, proton resonance frequency 400.13 MHz, ^1H, ^{13}C inverse 4 mm probehead with a ^2H–lock channel) and on the two spectrometers described above [proton resonance frequencies 200.13 MHz (4.7 T), 300.13 MHz (7.05 T)]. The chemical shifts were referenced with respect to TMS. The amount of sample employed was 20 mg in each cases. Deuterated NMR solvents were purchased from Cambridge Isotope Laboratories, Inc. and used

without further purification. The polysiloxanes were allowed to swell in the solvents at least for one hour in the 4 mm ZrO_2 rotors equipped with ceramic inserts. The rotation frequency was 4 kHz in all cases. The $T_{1\rho H}$ values in the suspended state were determined by a simple 90° single pulse excitation sequence with variation of the spin–lock time τ. Every experiment was performed with 16 scans.

6. References

[1] A. D. Pomogailo *Russ. Chem. Rev.* **1992**, *61*, 133.

[2] J. A. Marqusee, J. Dill *J. Chem. Phys.* **1986**, *85*, 434.

[3] L. C. Sander, S. A. Wise, In *Retention and Selectivity Studies in HPLC*; Smith, R. M., Ed.; Elsevier: Amsterdam, 1994, p 337.

[4] J. G. Dorsey, K. A. Dill *Chem. Rev.* **1989**, *89*, 331.

[5] E. Lindner, T. Schneller, F. Auer, H. A. Mayer *Angew. Chem.* **1999**, *111*, 2288; *Angew. Chem. Int. Ed.* **1999**, *38*, 2154.

[6] C. J. Brinker, G. W. Scherer, *Sol–Gel Science*; Academic Press: London, 1990.

[7] E. Lindner, M. Kemmler, H. A. Mayer, P. Wegner *J. Am. Chem. Soc.* **1994**, *116*, 348.

[8] L. L. Hench, J. K. West *Chem. Rev.* **1990**, *90*, 33.

[9] E. Lindner, R. Schreiber, M. Kemmler, T. Schneller, H. A. Mayer *Chem Mater.* **1995**, *7*, 951.

[10] U. Schubert, *New J. Chem.* **1994**, *18*, 1049.

[11] R. P. J. Corriu, D. Leclercq, *Angew. Chem.* **1996**, *108*, 1524–1540; *Angew. Chem. Int. Ed. Engl.* **1996**, *35*, 1420.

[12] F. R. Hartley, P. N. Vezey, *Adv. Organomet. Chem.* **1977**, *15*, 189.

[13] W. Dumont, J.–C. Poulin, T.–P. Dang, H. B. Kagan, *J. Am. Chem. Soc.* **1973**, *95*, 8295.

[14] E. Lindner, R. Schreiber, T. Schneller, P. Wegner, H. A. Mayer, W. Göpel, C. Ziegler, *Inorg. Chem.* **1996**, *35*, 514.

[15] E. Lindner, A. Jäger, T. Schneller, H. A. Mayer, *Chem. Mater.* **1997**, *9*, 81.

[16] E. Lindner, A. Jäger, F. Auer, P. Wegner, H. A. Mayer, A. Benez, D. Adam, E. Plies, *Chem. Mater.* **1998**, *10*, 217.

[17] E. Lippmaa, M. Mägi, A. Samson, G. Engelhardt, A.–R. Grimmer *J. Am. Chem. Soc.* **1980**, *102*, 4889. Q: quadrifunctional silicon; T: trifunctional silicon; D: difunctional silicon.

[18] E. Lindner, T. Schneller, H. A. Mayer, H. Bertagnolli, T. S. Ertel, W. Hörner, *Chem. Mater.* **1997**, *9*, 1524.

[19] E. Lindner, T. Schneller, F. Auer, P. Wegner, H. A. Mayer, *Chem. Eur. J.* **1997**, *3*, 1833.

[20] T. Schneller, Ph. D. Thesis, Univ. Tübingen 1997.

[21] E. Lindner, A. Baumann, P. Wegner, H. A. Mayer, U. Reinöhl, A. Weber, T. S. Ertel, H. Bertagnolli, *J. Mater. Chem.* **2000**, *10*, 1655.

[22] E. Lindner, W. Wielandt, A. Baumann, H. A. Mayer, U. Reinöhl, A. Weber, T. S. Ertel, H. Bertagnolli *Chem. Mater.* **1999**, *11*, 1833.

[23] E. Lindner, T. Salesch, F. Hoehn, H. A. Mayer *Z. Anorg. Allg. Chem.* **1999**, *625*, 2133.

[24] R. J. P. Corriu, J. Moreau, P. Thepot, M. Wong Chi Man, *Chem. Mater.* **1992**, *4*, 1217.

[25] G. Cerveau, R. J. P. Corriu, C. Lepeytre, *J. Organomet. Chem.* **1997**, *548*, 99.

[26] G. Cerveau, R. J. P. Corriu, C. Lepeytre, P. H. Mutin, *J. Mater. Chem.* **1998**, *8*, 2707.

[27] G. Cerveau, R. J. P. Corriu, C. Fischmeister–Lepeytre, *J. Mater. Chem.* **1999**, *9*, 1149.

[28] S. W. Carr, M. Motevalli, D. L. Ou, A. C. Sullivan, *J. Mater. Chem.* **1997**, *7*, 865.

[29] J. Zupan, J. Gasteiger, *Neural Networks for Chemists*; VCH Verlagsgesellschaft: Weinheim, 1993.

[30] A. Zell, *Simulation Neuronaler Netze*; Addison–Wesley: Reading, MA, 1994.

[31] D. E. Rumelhard, J. L. McClelland, *Parallel Distributed Processing: Explorations in the Microstructure of Cognition*; MIT Press: Cambridge, MA, 1986.

[32] T. Kohonen *Biol. Cybern.* **1982**, *43*, 59.

[33] C. A. Fyfe *Solid State NMR for Chemists*; CRC Press: Guelph, ON, 1984.

[34] C. A. Fyfe, Y. Zhang, P. Aroca *J. Am. Chem. Soc.* **1992**, *114*, 3252.

[35] H. Eckert *Prog. Nucl. Magn. Reson. Spectrosc.* **1992**, *24*, 159.

[36] R. Voelkel *Angew. Chem.* **1988**, *100*, 1525–1540; *Angew. Chem. Int. Ed.* **1988**, *27*, 1468.

[37] R. S. Aujla, R. K. Harris, K. J. Packer, M. Parameswaran, A. Say, A. Bunn, M. E. A. Cudby *Polym. Bull.* **1982**, *8*, 253.

[38] J. L. Koenig, M. Andreis, In *Solid State NMR of Polymers*; L. J. Mathias (Ed.), Plenum Press: New York, 1991; p 201.

[39] A. Abragam, *The principles of Nuclear Magnetism*; Clarendon Press: Oxford, 1961; pp 138, 139.

[40] H. W. Spiess *Chem. Rev.*, **1991**, *91*, 1321.

[41] V. J. McBrierty, D. C. Douglass *J. Polym. Sci., Part D: Macromol. Rev.* **1981**, *16*, 295.

[42] M. Mehring, *Principles of High–Resolution NMR in Solids*; Springer–Verlag: New York, 1983.

[43] D. A. McArthur, E. L. Hahn, R. E. Walstadt *Phys. Rev.* **1969**, *188*, 609.

[44] J. Schaefer, E. O. Stejskal, R. Buchdal *Macromolecules*, **1977**, *10*, 384.

[45] The degrees of condensation of the silyl species D, T and Q are calculated as following: $D = 100(D^1 + 2D^2)/[2(D^1 + D^2)]$; $T = 100(T^1 + 2T^2 + 3T^3)/[3(T^1 + T^2 + T^3)]$; $Q = 100(Q^1 + 2Q^2 + 3Q^3 + 4Q^4)/[4(Q^1 + Q^2 + Q^3 + Q^4)]$. D^1, D^2, T^1, etc., are the real signal intensities of the corresponding silylsubspecies in the ^{29}Si NMR spectra.

[46] L.–H. Tseng, D. Emeis, M. Rraitza, H. Händel, K. Albert *Z. Naturforsch.* **2000**, *55b*, 651.

[47] F. A. Bovey, *Nuclear Magnetic Resonance Spectroscopy*, 2nd ed., Academic Press, London, 1991, p 424.

[48] T. M. Alam, G. P. Drobny *Chem. Rev.* **1991**, *91*, 1545.

[49] H. W. Spiess, *Advances in Polymer Science 66*, Springer Verlag, Berlin, 1985, p 23.

[50] J. Göppert, *Die topologisch interpolierende selbstorganisierende Karte in der Funktionsapproximation*; Shaker Verlag, 1996; ISBN 3–8265–2401–2.

[51] A. Ultsch, In *Information and Classification*; O. Opitz, B. Lausen, R. Klar (Eds.), Springer–Verlag: New York, 1993; p 307.

[52] Unpublished results.

[53] a] J. Büchele, *Ph. D. Thesis*; Universität Tübingen, 1999; b] J. Büchele, H. A. Mayer *Chem. Commun.* **1999**, 2165.

[54] E. Lindner, S. Brugger, H. A. Mayer, manuscript in preparation.

[55] E. Lindner, F. Hoehn, T. Salesch, S. Singh, K. Müller, H. A. Mayer, manuscript in preparation.

[56] Personal communication by T. Salesch.

[57] The degree of hydrolysis of T/D copolymers is calculated as following: $100[(3T + 2D) - A(–OCH_3)/A(–CH_x–)]/(3T + 2D)$; T = real amount of T species in the polymer ; D = real amount of D species in the polymer; $A(–OCH_3)$ = peak area of the non hydrolyzed methoxysilyl or ethoxysilyl group in the ^{13}C CP/MAS NMR spectrum; $A(–CH_x–)$ = peak area of an unique functional group of the T species in the ^{13}C CP/MAS NMR spectrum. The degree of hydrolysis of pure D type polymers is calculated as following: $100[2 - A(Si–OCH_3)/A(Si–CH_3)]/2$; $A(Si–OCH_3)$ = peak area of the non hydrolyzed $Si–OCH_3$ group in the ^{13}C CP/MAS NMR spectrum; $A(Si–OCH_3)$ = peak area of the methyl group attached to the silicon atom in the ^{13}C CP/MAS NMR spectrum.

[58] The relative cross–linkage is equal to the average number of Si–O–Si bonds of a silyl group formed effectively in the polymer and is expressed as following for the D type polymers: RC = D(2/100) where RC is the relative cross–linkage, D is the degree of condensation of the D groups. For the T type polymers it is: RC = T(3/100), T is the degree of condensation of the T groups.

[59] Personal commnication by S. Singh.

[60] K. Schmidt–Rohr, J. Clauss, H. W. Spiess *Macromolecules* **1992**, *25*, 3273.

[61] G. Cerveau, J. P. Corriu, E. Framery *J. Mater. Chem.* **2000**, *10*, 1617.

7. Summary

Specially designed sophisticated polymers are applied in wide areas of chemistry today, and are implemented for example in chromatography, solid phase synthesis, or for biochemical and medical purposes (micro or nano filters, dialysis). In most of these applications the polymers act as a 'passive' support for the reactive centers which are actively performing what they are assigned to do. In chemistry in interphases the polymeric matrix is more than only a support for the reactive centers (e.g. transition metal complexes). The polymer with the uniformly incorporated reactive centers is an entity. This means that the overall (mechanical, physical, and chemical) properties of these inorganic–organic hybrid polymers have to be taken into account when rating their value, e.g. in catalytic reactions. The synthesis of siloxane–based inorganic–organic hybrid polymers is carried out by sol–gel processing of alkoxysilyl functionalized co–condensing agents (**D^0**, **T^0**, **Q^0**, or recently developed **D^0–C_z–D^0**, **D^0–$(CH_2)_z$–C_6H_4–$(CH_2)_z$–D^0** monomers, etc.) with trimethoxysilyl–(T)–functionalized ligands or transition metal complexes. This reaction type provides mild and reproducible conditions and yields xerogels of homogeneous composition and of completely amorphous nature. The properties of the polymeric matrix depend highly on the way the sol–gel process is carried out (employed solvent, concentration of the educts, temperature, etc.). The acquirement of profound knowledge of these properties (swelling abilities, mobilities in the dry state and in the interphase, cross–linkage) is of great importance prior these functionalized siloxanes are employed in chemical reactions.

The first part of this thesis deals with solid state NMR spectroscopic characterizations and mobility studies of siloxane–based inorganic–organic hybrid polymers, that were recently synthesized by *T. Salesch*. These investigations were carried out in the dry and the suspended state. In the second part of this work – in cooperation with *T. Hermle*, a member

of the computing faculty of the University of Tübingen – the application of an Artificial Neural Network in the evaluation of a large number of inorganic–organic hybrid polymers is described, that were synthesized earlier by other members of this group. The motivation for this task is the attempt to compare the properties of these polymers which can not be done with conventional statistical methods, like principle component analysis. Although the structural and dynamic features of these polymers are quite different, similarities are present, since these compounds were synthesized by comparable sol–gel routes. The data basis for the evaluation consists of solid state NMR spectroscopic derived dynamic parameters and is analyzed by the so called Self–Organizing Feature Map, that was first implemented by Kohonen.

The ^{13}C and ^{29}Si solid state NMR spectroscopic characterizations of the inorganic–organic hybrid polymers revealed the structural integrity of the polymeric matrix after sol–gel processing. The formation of homogeneous composed copolymers was confirmed by the determination of only one value for $T_{1\rho H}$. This is in favor for a uniform relaxation process of the nuclear spins, controlled by spin–diffusion. It was demonstrated that the initial stoichiometries of the D and T type monomers were retained after sol–gel processing. This was a very important finding, since it is planned to employ $\mathbf{D^0–(CH_2)_3–C_6H_4–(CH_2)_3–D^0}$ frequently as a co–condensing agent in chemistry in interphases. The polarity of the solvents which are used in the sol–gel processes has a large influence on the properties of the resulting xerogels. For example the application of MeOH leads to polymers with medium to low degrees of condensation, especially concerning only D type polymers. Materials with high cross–linkage are obtained if THF is employed. This fact has direct consequences for the mobilities of these polymers since a lower cross–linkage leads to an increased mobility, and vice versa. The same was found for mixed D/T type copolymers.

The mobilities of the inorganic–organic hybrid polymers in the dry state were studied by determinations of $T_{1\rho H}$ in dependence on the temperature. The deuterated polymers were additionally investigated by dynamic ^2H NMR spectroscopy. The temperature dependent investigations of $T_{1\rho H}$ allow only qualitative comparisons of the mobilities of the polymers. Furthermore, a direct comparison of the mobilities of only D or only T type polymers with regard to $T_{1\rho H}$ is difficult and has to be carried out carefully. In this case particularly the relative cross–linkage of these polymers has to be taken into account. A strong dependence of cross–linking on the solvent employed in the sol–gel process – and of mobility on cross–linkage – is found, regarding all investigated polymers. The exploration of the deuterated compounds by dynamic deuteron NMR spectroscopy additionally revealed an absolute order concerning their mobility: the D type matrixes were definitely more mobile that the T type ones. Furthermore, the MeOH sol–gel process derived polymers were more mobile than the THF derived materials, caused by the lower cross–linkage.

NMR spectroscopy in the interphase (in suspensions of MeOH, THF, and DCM) first of all revealed the swelling abilities of the investigated polymers. It was found that swelling depends on the type of the silyl species rather than on the degrees of condensation. Cross–linkage is the second important criterion for the swelling capability. In all cases the ^1H NMR spectra of D type polysiloxanes provided good resolved signals that could be analyzed in order to determine the $T_{1\rho H}$ values in the interphase. T type polymers swell little and the spectra recorded of their interphases resemble often solid state NMR spectra. In these cases determinations of $T_{1\rho H}$ were difficult and sometimes not advisable. Nevertheless, the T type polysiloxanes with the lowest degrees of condensation at all and especially the mixed type copolymers could be investigated and afforded unequivocal $T_{1\rho H}$ values for their different proton sites. In the suspended state the proton

sites of all investigated polysiloxanes relax at different rates. This is the result of the increased mobility of the molecular fragments and therefore decreasing dipole–dipole interactions between the proton spins. Different mobilities for different functional sites in the polymers are detected. It was found that terminal functionalities such as methyl, methoxy, or ethoxy groups were most mobile, followed by methylene groups in the middle of aliphatic chains. Surprisingly triphenylphosphine fragments in copolycondensates reveal a similar mobility as the corresponding non–hydrolyzed ethoxy groups.

In the second part of this thesis the attempt of a classification of inorganic–organic hybrid polymers by a neural network is described. The evaluated materials comprise sol–gel processed transition metal complexes as well as ligands of different shapes and geometries. Furthermore different co–condensing agents were used to generate these stationary phases. The analysis was performed on the basis of NMR spectroscopic derived dynamic parameters, such as the relaxation times $T_{1\rho H}$ (determined via ^{29}Si and ^{31}P CP/MAS NMR spectroscopy), the cross–polarization constant T_{PH} and the degrees of condensation of the corresponding silyl species. The employed neural network is a Self–Organizing Feature Map (SOM), also called Kohonen Map. This is an unsupervised learning, topology and neighborhood relationship preserving neural network and is best suited for classification purposes – in this case for the search of similarities between the evaluated compounds. The results of this analysis were visualized by two–dimensional maps and supported by corresponding distribution maps of the most important dynamic parameters. It was found that the neurons on the large Kohonen map are divided into three areas that contain the polysiloxanes in dependence on the type of the silyl species co–condensed with the complexes or the ligands – the D–, T–, and Q–domains. Within the domains the compounds are 'sorted' depending on commonly shared main features. The most important parameters seem to be the cross–polarization constant T_{PH} and the relaxation times $T_{1\rho H}$ as they represent the mobility of the polysiloxanes. The other parameters are of minor

importance and it is not easy to judge their influence on the placement of the compounds on the Kohonen map. This means that the macromolecular properties of the polymers are the dominant features that take a decision on the positions of the compounds on the map. Properties such as shape or geometry are subordinate. Regarding the structural features of these polymers, it was demonstrated that the educts must be provided with an aliphatic chain acting as a spacer, to gain mobility. The exact location of this spacer is less important and can be adapted to the necessities of synthesis.

Meine akademische Ausbildung verdanke ich:

K. Albert, E. Bayer, M. Brendle, D. Christen, H. Clement, H. Eckstein, H.–J. Egelhaaf, G. Gauglitz, J. Gelinek, W. Göpel, G. Häfelinger, M. Hanack, D. Hoffmann, V. Hoffmann, G. Jung, W. Koch, B. Koppenhöfer, D. Krug, E. Lindner, I.–P. Lorenz, H. A. Mayer, U. Nagel, P. W. Nakel, H. Oberhammer, D. Oelkrug, H. Pauschmann, G. Pausewang, H. Pommer, B. Rieger, A. Rieker, V. Schurig, E. Schweda, F. F. Seelig, H.–U. Siehl, H. Stegmann, J. Strähle, K.–P. Zeller, C. Ziegler

Lebenslauf

Persönliche Daten:

Name:	Frank Höhn
Geburtsdatum/–ort:	28. August 1967 in Waiblingen (Rems–Murr–Kreis)
Eltern:	Peter Höhn, Herta Höhn, geb. Becker
Staatsangehörigkeit:	deutsch

Schulbildung:

09/74 – 08/78	Grundschule Stuttgart/Ostheim
09/78 – 08/85	Königin–Katharina–Stift Gymnasium Stuttgart
09/85 – 07/87	Wagenburg Gymnasium Stuttgart
02.06.1987	Abitur

Zivildienst:

01/88 – 08/89	Zivildienst i. d. ev. Kirchengemeinde Stuttgart/Rot

Studium:

10/89	Beginn des Diplomstudiengangs Chemie a. d. Eberhard–Karls–Universität Tübingen
07.04.1992	Diplomvorexamen
15.07.1996	Mündliches Diplomhauptexamen
08/96 – 02/97	Diplomarbeit mit dem Titel: "Sol–Gel–prozessierte (Ether–phosphan)ruthenium(II)–Komplexe: Vergleich unterschiedlicher Darstellungen und Charakterisierung durch Festkörper–CP/MAS–NMR–Spektroskopie" unter Anleitung von Prof. Dr. E. Lindner, am Institut für Anorganische Chemie der Universität Tübingen
12.02.1997	Zeugnis über die Diplomreife in Chemie
04/97 – 12/00	Dissertation mit dem Titel "Mobilitätsstudien an anorganisch–organischen Hybridpolymeren auf Siloxanbasis mittels Techniken der hochauflösenden Festkörper– und Suspensions–NMR Spektroskopie und Analyse NMR–spektroskopisch ermittelter dynamischer Parameter mit Hilfe eines Neuronalen Netzwerkes" unter der Leitung von Prof. Dr. E. Lindner am o. g. Institut.